Angewandte Chemie
Eine Zeitschrift der Gesellschaft Deutscher Chemiker

Supporting Information

Aptamers with Tunable Affinity Enable Single-Molecule Tracking and Localization of Membrane Receptors on Living Cancer Cells

Pietro Delcanale[+], David Porciani[+], Silvia Pujals, Alexander Jurkevich, Andrian Chetrusca, Kwaku D. Tawiah, Donald H. Burke, and Lorenzo Albertazzi**

anie_202004764_sm_miscellaneous_information.pdf

Supporting Information

Table of Contents

Experimental Procedures

Materials

All chemicals were purchased from Sigma-Aldrich (St Louis, MO, USA) unless otherwise noted. Cell culture products were purchased from Gibco BRL/Life Technologies (Gaithersburg, MD, USA). Stock solution of sheared salmon sperm DNA (sssDNA) at 10 mg/mL was purchased from Invitrogen and aliquots were stored at -20°C. EGFR monoclonal antibody (clone 199.12) from mouse and anti-mouse secondary antibody conjugated to AlexaFluor647 were purchased from ThermoFisher (Waltham, MA).

Cell culture

A431 and MCF-7 cells were purchased from the American Type Culture Collection (ATCC, Manassas, VA) while MD-MBA-231 cells were gifted by Dr. Vito Conte, Institute for Bioengineering of Catalonia. A431, MCF-7 and MD-MBA-231 cells were cultured in DMEM supplemented with 10% Fetal Bovine Serum (FBS), 100 U/mL Penicillin and 100 µg/mL Streptomycin. Cells were cultured at 37°C with 5% CO_2 and passed when confluent. HeLa cells were gifted by Dr. Christian Lorson, University of Missouri-Columbia. A549 cells were gifted by Dr. Bumsuk Hahm, University of Missouri-Columbia. HEK293T cells and Ramos cells were purchased from the ATCC. HeLa and HEK293T cells were cultured in DMEM containing 1 mM sodium pyruvate, 2mM L-glutamine, and 10% FBS. A549 cells were cultured in DMEM containing 1 mM sodium pyruvate, 2mM L-glutamine, 100 U/ml penicillin and 100 µg/ml streptomycin (ThermoFisher, Waltham, MA), and 10% Bovine Calf Serum (BCS). Ramos cells were cultured in RPMI 1640 medium containing 1 mM sodium pyruvate, 2 mM L-glutamine, supplemented with 10% BCS. Cells were maintained at 37°C in a humidified 5% CO_2 atmosphere. For imaging experiments with A431, MDA-MBA-231 and MCF-7 cell lines, cells were seeded in LabTek 8-well chamber slides (Nunc 155411) at 15,000 cells/well and incubated overnight in culture medium. For imaging experiments with HeLa and A549 cell lines, cells were seeded 48 hours before the imaging onto glass-bottom petri dishes (WillCo-dish GWST-3512) at 10,000 cells/dish. Cells were incubated in complete medium. Then, 12 hours before the imaging, cells were washed once with DPBS and fresh 2% serum-containing medium was added.

DNA Templates, list of primers and RNA Transcription

All DNA oligos were purchased from Integrated DNA Technologies (IDT, Coralville, IA, USA) and resuspended in the appropriate volume of TE buffer (10 mM Tris-HCl pH 8.0, 1 mM EDTA) to reach a stock concentration of 100 µM. All 2′F-pyrimidine-modified RNA aptamers included an extended 'tail' sequence (5'-GCAGCAGCAGCAGCAGCAGCA-3'). For live-cell imaging, complementary DNA anti-tail (5'-TCGTCGTCGTCGTCGTCGTCGT-3') was purchased from IDT DNA Technologies directly conjugated to either Atto647N or AF488 at its 3-end. For flow cytometry experiments, Cy5-labeled DNA anti-tail was generated following a protocol previously described[1]. In brief, a 5'-aminohexyl-modified DNA anti-tail (IDT, Coralville, IA) was first coupled to Cy5-NHS ester, and then Cy5-labeled DNA anti-tail was purified by RP-HPLC and concentrated using spin desalting column (Amicon Ultra-0.5 mL, 3K MWCO). Same protocol was also used to couple ATTO647N-NHS ester to the 5'-aminohexyl DNA anti-tail, thus generating a 5'-modified ATTO647N-anti-tail that was used for live-cell PAINT shown in Figure S12 and S13.

2′F-pyrimidine-modified RNA aptamers were generated via *in vitro* run-off transcription. First, the corresponding DNA templates were PCR amplified with primers that appended a T7 promoter (list of templates and primers is reported in Table S3). Then, 2′F-pyrimidine-modified RNA aptamers were transcribed by run-off transcription reaction (overnight at 37°C) using a recombinant mutant form of T7 RNA polymerase (Y639F mutant), *in vitro* transcription buffer (50 mM Tris-HCl pH 7.5, 15 mM $MgCl_2$, 5 mM DTT, 4% w/v PEG4000 and 2 mM spermidine), and 2 mM of each ATP, GTP, 2'-fluoro modified CTP and 2'-fluoro modified UTP (TriLink Biotechnologies, San Diego, CA, USA). All RNA aptamers were purified through denaturing polyacrylamide gel electrophoresis (0.75 mm, 8% TBE-PAGE, 8 M urea) and bands corresponding to the expected product size were gel extracted and eluted while tumbling overnight in 300 mM Sodium Acetate pH 5.4. Eluates were ethanol precipitated, resuspended in TE buffer, and stored at −20°C until further use.

Aptamer folding and annealing with dye-labeled DNA oligo

SUPPORTING INFORMATION

In vitro annealing reactions were prepared at room temperature in "cell-binding buffer" (Dulbecco's phosphate buffered saline, DPBS pH 7.4 supplemented with 5 mM $MgCl_2$) using a slight excess of RNA aptamer over the dye-labeled anti-tail (2:1 molar ratio of aptamer-tail:anti-tail). For thermal renaturation, samples were transferred into a preheated aluminum insert within a dry heat block set to 90°C. Samples were kept at 90°C for 1 minute to denature nucleic acid structures, and then the aluminum insert was removed from the block heater and placed on the workbench to cool down to 37°C. This slow cooling process enables proper aptamer folding and correct hybridization between aptamer-tail and dye-labeled anti-tail. For live-cell imaging experiments, dye-conjugated aptamer samples were always freshly prepared before each experiment at 5x concentration, unless otherwise noted. After annealing, aptamer samples (5x) were then further diluted in "Live Cell Imaging Solution" pH 7.4 (Invitrogen) to the final concentration used for live-cell imaging. All dye-conjugated aptamer concentrations are indicated in the figure legends. sssDNA, a competitor for non-specific binding sites, was added to each sample at a final concentration of 1.0 mg/ml. Concentration of $MgCl_2$ was adjusted to keep a final concentration of 5 mM Mg^{2+}.

Flow cytometry assay

To determine aptamer binding, each cell line (HeLa, HEK293T and Ramos cells) was seeded at 30,000-50,000 cells/well in a 48-well flat bottom tissue culture plate two days before the flow cytometry experiment. Following the protocol described above, aptamer-tail were folded and annealed to Cy5-anti-tail in cell-binding buffer at 2x concentration. After annealing reactions, aptamer solutions (2x) were diluted to 1x concentration with cell-binding buffer supplemented with sssDNA (1.0 mg/ml). Concentrations of Cy5-aptamers are reported in the figure legends (Fig.S4-S8). Cells were washed twice with DPBS, and then were incubated for 1h at 37°C with Cy5-aptamers. Upon 1h incubation, medium was removed, and cells were washed with 200 µl DPBS. In the case of adherent cell lines (HeLa and HEK293T), cells were lifted with 150 µl 1X Tryple Express (ThermoFisher, Waltham, MA) for 3–5 minutes at 37°C, followed by addition of 500 µl of complete medium. For all cell lines, cell suspensions were transferred into 1.5 mL conical tubes and briefly centrifuged (400 xg, 3–5 min) to pellet cells. After resuspension in 200 µl of 4% paraformaldehyde in 1X DPBS, cells were fixed for 5 minutes at 4°C in the dark, and then were pelleted by centrifugation. Finally, cell pellets were resuspended in DPBS supplemented with 2 mM $MgCl_2$. Flow cytometry was performed on a BD Accuri C6 (BD Biosciences, San Jose, CA, USA) counting 20,000-30,000 live cell events. Cy5 fluorescence was excited using a 640 nm laser and detected using a standard FL-4 filter [675±12.5 nm]. Flow cytometry data were then analyzed and processed using FlowJo Software (Treestar, Ashland, OR, USA). Viable cells were gated and analyzed, while dead cells (typically < 10%) were identified by the forward scatter plot and excluded from the analysis.

For binding assays in presence of specific or non-specific competitors ((MinE07 and CD4BA, respectively), Cy5-conjugated aptamers were prepared as described above at 2x concentration (100 nM). In separate tubes, aptamer competitor samples were annealed to free DNA anti-tail (with no fluorophore) at 2x concentration (1,000 nM). Then, individual Cy5-aptamer samples and their corresponding competitors were combined to form final samples that included sssDNA (1.0 mg/ml). HeLa cells were incubated for 1h at 37°C in 180 µl of Cy5-aptamer samples 50 nM (± aptamer competitor 500 nM), and aptamer staining was investigated as described above.

Determination of apparent dissociation constant ($K_{D\ app}$)

Data analysis from titration experiments were analyzed using GraphPad Prism 6 (GraphPad Software, La Jolla, CA). Median fluorescence Intensity (MFI) values obtained using increasing concentrations of Cy5-CD4BA were used as background, and subtracted to the MFIs obtained with cell-targeting aptamers (Waz, high-affinity MinE07, and low-affinity MinE07). Apparent dissociation constants ($K_{D\ app}$) for each aptamer were determined applying nonlinear regression analysis by fitting the experimental data with the "one-site specific binding" equation: $Y = Bmax*X/(K_D + X)$. R square values of the fitting shown in Fig.S8 were 0.94, 0.85, and 0.95 for Waz, High-affinity MinE07, and low-affinity MinE07, respectively. $K_{D\ app}$ values reported in Fig.3b were obtained from a minimum of three independent experiments.

Optical setup

Single-molecule imaging was performed with a Nikon N-STORM system configured for total internal reflection (TIR) and endowed with Perfect Focus System for axial drift correction. Three continuous excitation lasers were used (values in parentheses represent maximum power for each laser): 488 nm (80 mW, 0.9 kW/cm^2), 561 nm (80 mW, 0.9 kW/cm^2), or 647 nm (160 mW, 1.9 kW/cm^2). Upon laser excitation, fluorescence was collected by a 100x 1.49 NA oil-immersion objective, passed through a quad-band dichroic mirror (97335 Nikon), and was finally detected by a Hamamatsu ORCA Flash 4.0 CMOS camera with 160 nm pixel size. The signal was collected on a 256x256 pixel region, without binning, allowing the detection of 40 µm sized images. Microscope was equipped with an incubator for live-cell imaging, with temperature controller and a CO_2-air gas mixer system (OkoLab).

Live-cell imaging of HeLa and A549 cells (Fig.SN2) was performed at room temperature on a Leica SR GSD 3D microscope using a 160x objective lens (HC PL APO 160x/1.43, oil immersion), a 500-mW 642 nm laser (MPBC Inc., Montreal, Quebec, Canada), a 710/100 nm emission bandpass filter, and a EMCCD camera (iXon Ultra 897, Andor, UK). The microscope was equipped with the TIRF scanner allowing azimuthal selection of the wavefront of the evanescent wave. TIRF illumination was applied with penetration depth in the range 160–200 nm and azimuthal direction of the illumination beam of 180°. Fluorescence signal was collected on a 512x512 pixel region with 99 nm pixel size.

Live single-cell imaging with fluorescently-conjugated aptamers

SUPPORTING INFORMATION

Microscope incubator was maintained at 37°C and with 5% CO_2 air flow during experiments. Prior to imaging, cells were washed 3 times with pre-warmed PBS buffer to remove culture medium before adding the aptamer-containing solution. Cells in each well of the chamber were washed and imaged sequentially. Total internal reflection (TIR) irradiation was always employed.

SMT results of Fig.2a-c and Fig.S1-S2 were obtained from movies acquired at different sampling frequencies: each frame acquired using the excitation laser was preceded by 1-6 dark frames (no irradiation), successively discarded. Movies were acquired with 60 ms camera exposure time and attenuated excitation: 20% or 40% of maximum power, for 647 nm and 488 nm lasers respectively. The rather long exposure time (60 ms) was necessary to well-localize single molecules under the low excitation power employed. 300 frames movies of the same cell were acquired with the 6 sampling frequencies (120-420 ms periods), corresponding to a total acquisition time of 36-126 s. Lateral drift of the sample was not significant over this time. Prior to every acquisition, the sample was kept in the dark for 3 min in order to restore identical initial conditions. Two movies were acquired for each sampling frequency on 3 different cells in separate experiments. The representative trajectories shown Fig. 2b-c were acquired with 240 ms sampling period.

Two-color SMT results of Fig.2d-f were obtained from movies acquired alternating 1-frame of 647 nm and 1-frame of 488 nm laser excitation, attenuated at 20% and 40% of maximum power respectively. Movies of 300 frames were acquired with a camera exposure time of 60 ms, for a total acquisition time of 36 s. Measurements were repeated 3 times on 5 different cells.

PAINT images of Fig.3, Fig.S10, Fig.S12, Fig.4a-c and Fig.5a and trajectory maps of Fig.5b-e, Fig.S14 and Fig.S15 were obtained from movies of 10000 consecutive frames, with a camera exposure time of 50 ms, using 647 nm laser excitation at 50% of maximum power.

For live-cell imaging on HeLa cells shown in Fig. SN2a, Atto647N-aptamer samples were prepared as describe above. However, for imaging in live HeLa and A549 cells (Fig. SN2b-c) performed in presence of macromolecular crowding agent (Dextran Sulfate), the labeling protocol was slightly changed as follows. In brief, aptamer-tail samples were folded and annealed to Atto647N-anti-tail at 5x concentration (100 nM) as described above. Cells were first incubated for 10 minutes with cocktail of polyanionic competitors that include: sssDNA (1 mg/ml), Dextran Sulfate (500 kDa, 1 mg/ml), and an arbitrary 2′F-pyrimidine-modified RNA (2 μM) (5'-GGGAAAAGCGAAUCAUACACAAGAAAUUUGGACUUUCCGCCCUUC-3'). Then, 40 μl of aptamer solution (5x) were added directly to the cells while still incubated with 160 μl cocktail of competitors. Cells were imaged about five minutes after the aptamer addition. PAINT images of Fig.SN2a-c were obtained from movies of 5000 consecutive frames recorded using a Leica SR GSD 3D (see above for further details) with a camera exposure time of 50 ms, using 642 nm laser excitation at 40% of maximum power.

Single-molecule tracking analysis

Diffraction limited movies were analyzed with the software ImageJ using the plugin Particle Tracker 2D/3D developed by MOSAIC group[2]. Briefly, the algorithm detects in every frame the positions of intensity maxima corresponding to individual emitters, according to user-defined parameters of size and intensity. Then, the positions are linked to reconstruct trajectories with a user-defined maximum displacement value between consecutive frames that was set according to the features of the sample. Additionally, a gap of at most 1 frame in the reconstruction of the trajectory was allowed. This was essential to correct for the possibility that a molecule being tracked might be transiently not recognized for 1-frame by the algorithm. Two-dimensional diffusion coefficient (D) values were calculated by the software, assuming a Brownian motion model, for trajectories longer than 5-frames and considering the initial one-third portion of the trajectory. Additionally, diffusive regimes can be discriminated by the slope of the moment scaling spectra (MSS) analysis, provided by the software. D value distributions obtained from movies at different sampling frequencies and on different A431 cells resulted very consistent and were then merged to obtain the distribution shown in Fig. 2a.

PAINT image reconstruction and measurements of localization density

For live-cell PAINT imaging shown in Fig.3, Fig.S10, Fig.S12, Fig.4a-c and Fig.5a, images were reconstructed using the analysis tool of NIS-elements software from Nikon. This generates a list of localizations by Gaussian fitting the single-molecule fluorescence spots in each frame of the acquired diffraction-limited movie. The first 700 frames of the acquisition, which are necessary for an equilibration of the localization rate, were not considered. Correction for the lateral drift occurring during acquisition was performed using a tool in the NIS-elements software, based on an autocorrelation algorithm. Single-molecule localizations in the reconstructed image were counted within selected Regions Of Interest (ROIs) using the “ROI-statistics” tool in the software, which reports area and number of single-molecule localizations, to calculate the localization density. Comparison of localization densities, reported in Fig.4d, resulted from 10 repetitions on different cells obtained in 2 separate experiments.

To reconstruct live-cell imaging data on HeLa and A549 cells shown in Fig.SN2, stacks of 5000 frames (512x512 pixels) were analyzed using ThunderSTORM plugin for ImageJ[3] according to the parameters reported in figure legend of Fig.SN2. Reconstructions were generated using Normalized Gaussian at a magnification of 15x. A ‘green’ LUT was applied before exporting the images as 32 bit RGB TIFFs. The list of localizations of the single emitters obtained with ThunderSTORM was used to calculate localization densities in selected ROIs (3.25 x 3.25 μm) of the reconstructed PAINT images. For each aptamer sample, in areas with cells, four ROIs were measured in three different fields of view for two independent experiments (total 24 ROIs). Similarly, localization density on the glass coverslip was measured in three ROIs in areas with no cells, in three fields of view for two independent experiments (total 18 ROIs).

Trajectories density maps

Trajectory density maps reported in Fig.5b-e and Fig.S14 and Fig.S15 were constructed from SMT results. First, SMT analysis was performed as described above, with a careful optimization of user-defined parameters, resulting from systematic screening, to avoid trajectory overlap. Results of the SMT analysis were then further processed using a custom script in Matlab. Briefly, each retrieved trajectory longer than 5-frames (X-Y-T coordinates) was first associated to the corresponding diffusion parameters calculated by the

software, *e.g.* D and distance covered. A few trajectories, ~1% of the total, showing unrealistic motion ($D < 5 \cdot 10^{-6}$ $\mu m^2/s$ or $D > 10$ $\mu m^2/s$) were discarded. For the selection of sub-populations, trajectories were further filtered according to user-defined range of D or distance covered. After the filtering, spatial coordinates of the mass centers were calculated for each trajectory and binned in two-dimensions using a user-defined binning size. The 2D matrix obtained from the binning, corresponding to the trajectory density map, was then plotted using a colorimetric code. The density of trajectories within a region of interest was easily obtained from the map.

STORM imaging on fixed cells

Living cells from the same LabTek chamber used for PAINT experiments, but not exposed to aptamers, were washed 3-times with PBS and then fixed with 4% paraformaldehyde at room temperature for 15 min. Cell were then washed and blocked using 0.3 M of Glycine (15 min) and 30 mg/mL of BSA (30 min), washed again and stored in PBS at 4ºC. Immunostaining was performed on a different day: cells were first incubated with 5 µg/mL of monoclonal anti-EGFR antibody from mouse with 10 mg/mL BSA (2 h), washed 3-times and then incubated with 20 µg/mL of secondary anti-mouse antibody conjugated with AlexaFluor647 (2h), washed and imaged immediately. STORM imaging was performed in freshly prepared imaging buffer (PBS with glucose oxidase 0.5 mg/mL, catalase 40 µg/mL, glucose 5% w/v and cysteamine 100 mM) that promoted fluorophore blinking. Movies were recoded with 647 nm laser excitation (at maximum power) for 20,000 consecutive frames using 10 ms camera exposure time and then analyzed with NIS-elements software to reconstruct the STORM images of Fig.S11.

SUPPORTING INFORMATION

Supplementary Tables

Table S1. Cell lines used in this study listed according to the levels of expression of EGFR as reported in the literature. Corresponding citations that described EGFR (or TfR) levels in each cell line are included in the main text.

Cell line	Levels of expression (receptor/cell)	Type of cell
A431	10-30 x 10^5 EGFR 2-4 x 10^5 TfR	Epidermoid carcinoma (skin cancer)
A549	2-3 x 10^5 EGFR	Non-small cell lung cancer
MDA-MB-231	1-3 x 10^5 EGFR	Breast cancer
HeLa	1-2 x 10^5 EGFR	Cervical cancer
HEK293T	0.05-0.1 x 10^5 EGFR	Embryonic kidney
MCF-7	0.01-0.05 x 10^5 EGFR	Breast cancer
Ramos	EGFR-negative	B cell lymphoma

Table S2. List of aptamer sequences used in this study.

Note that among the seven MinE07 variants, some were designed according to aptamer sequences reported together with E07 (full-length parent of MinE07) during the original in vitro selection [See ref 24 in main text]

MinE07 aptamer variants		
Aptamer name [b]	Sequence 5' to 3' [a] (mutations are highlighted in red)	Minimum Free Energy ΔG (kcal/mol)[b]
MinE07	GGACGGAUUUAAUCGCCGUAGAAAAGCAUGUCAAAGCCGGAACCGUCC	-10.70
MinE07_A3U	GG**U**CGGAUUUAAUCGCCGUAGAAAAGCAUGUCAAAGCCGGAACCGUCC	-6.80
MinE07_U46A	GGACGGAUUUAAUCGCCGUAGAAAAGCAUGUCAAAGCCGGAACCG**A**CC	-5.30
MinE07_C4A/U46A	GGA**A**GGAUUUAAUCGCCGUAGAAAAGCAUGUCAAAGCCGGAACCG**A**CC	-3.90
MinE07_C4A/G45A /U46A	GGA**A**GGAUUUAAUCGCCGUAGAAAAGCAUGUCAAAGCCGGAACC**AA**CC	-3.20
MinE07_G6U	GGACG**U**AUUUAAUCGCCGUAGAAAAGCAUGUCAAAGCCGGAACCGUCC	-6.70
MinE07_G6U/U46A	GGACG**U**AUUUAAUCGCCGUAGAAAAGCAUGUCAAAGCCGGAACCG**A**CC	-5.30
MinE07_G6U/A33C	GGACG**U**AUUUAAUCGCCGUAGAAAAGCAUGUC**C**AAGCCGGAACCGUCC	-8.70
Additional aptamer sequences		
Waz-tail	GGGUUCUACGAUAAACGGUUAAUGACCAGCUUAUGGCUGGCAGUUCCCCGACGACGACGACGACGACGA	
CD4BA-tail	GGGAGACAAGAAUAAACGCUCAAUGACGUCCUUAGAAUUGCGCAUUCCUCACACAGGAUCUUUUCGACAGGAGGCUCACAACA GGCCGACGACGACGACGACGACGA	
Anti-tail	TCGTCGTCGTCGTCGTCGTCG	

[a] Note that all MinE07 sequences were tested with an extended tail sequence (CGACGACGACGACGACGACGA) annealed to its complementary anti-tail as reported for Waz and CD4BA (see sequences underlined). [b] MinE07 and MinE07_G6U/A33C are also referred to in the main text as "high-affinity MinE07" and "low-affinity MinE07, respectively.

SUPPORTING INFORMATION

Table S3. List of DNA templates (shown as sense strands) and primers used in this study.

	Sequences (5' to 3')
MinE07 template	GGACGGATTTAATCGCCGTAGAAAAGCATGTCAAAGCCGGAACCGTCCCGACGACGACGACGACGACGA
MinE07 forward primer	GGATAATACGACTCACTATAGGACGGATTTAATCGC
MinE07 reverse primer	TCGTCGTCGTCGTCGTCGTCGGG
MinE07_A3U template	GGTCGGATTTAATCGCCGTAGAAAAGCATGTCAAAGCCGGAACCGTCCCGACGACGACGACGACGACGA
MinE07_A3U forward primer	GGATAATACGACTCACTATAGGTCGGATTTAATCGC
MinE07_A3U reverse primer	TCGTCGTCGTCGTCGTCGTCGGG
MinE07_U46A template	GGACGGATTTAATCGCCGTAGAAAAGCATGTCAAAGCCGGAACCGACCCGACGACGACGACGACGACGA
MinE07_U46A forward primer	GGATAATACGACTCACTATAGGACGGATTTAATCGC
MinE07_U46A reverse primer	TCGTCGTCGTCGTCGTCGTCGGGTCG
MinE07_C4A/U46A template	GGAAGGATTTAATCGCCGTAGAAAAGCATGTCAAAGCCGGAACCGACCCGACGACGACGACGACGACGA
MinE07_C4A/U46A forward primer	GGATAATACGACTCACTATAGGAAGGATTTAATCGC
MinE07_C4A/U46A reverse primer	TCGTCGTCGTCGTCGTCGTCGGGTCG
MinE07_C4A/G45A/U46A template	GGAAGGATTTAATCGCCGTAGAAAAGCATGTCAAAGCCGGAACCAACCCGACGACGACGACGACGACGA
MinE07_C4A/G45A/U46A forward primer	GGATAATACGACTCACTATAGGAAGGATTTAATCGC
MinE07_C4A/G45A/U46A reverse primer	TCGTCGTCGTCGTCGTCGTCGGGTTG
MinE07_G6U template	GGACGTATTTAATCGCCGTAGAAAAGCATGTCAAAGCCGGAACCGTCCCGACGACGACGACGACGACGA
MinE07_G6U forward primer	GGATAATACGACTCACTATAGGACGTATTTAATCGC
MinE07_G6U reverse primer	TCGTCGTCGTCGTCGTCGTCGGG
MinE07_G6U/U46A template	GGACGTATTTAATCGCCGTAGAAAAGCATGTCAAAGCCGGAACCGACCCGACGACGACGACGACGACGA
MinE07_G6U/U46A forward primer	GGATAATACGACTCACTATAGGACGTATTTAATCGC
MinE07_G6U/U46A reverse primer	TCGTCGTCGTCGTCGTCGTCGGGTCG
MinE07_G6U/A33C template	GGACGTATTTAATCGCCGTAGAAAAGCATGTCCAAGCCGGAACCGTCCCGACGACGACGACGACGACGA
MinE07_G6U/A33C forward primer	GGATAATACGACTCACTATAGGACGTATTTAATCGC
MinE07_G6U/A33C reverse primer	TCGTCGTCGTCGTCGTCGTCGGG
Waz template	GGGTTCTACGATAAACGGTTAATGACCAGCTTATGGCTGGCAGTTCCCCGACGACGACGACGACGACGA
Waz forward primer	TAATACGACTCACTATAGGGGTTCTACGAT
Waz reverse primer	TCGTCGTCGTCGTCGTCGTCGGGGAACTGCCAG

SUPPORTING INFORMATION

Supplementary Figures

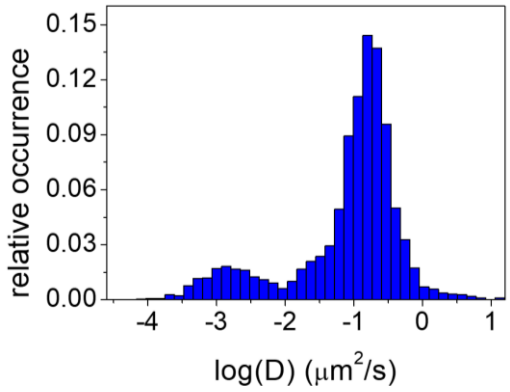

Figure S1. Distribution of the diffusion coefficient values measured from single-molecule tracking analysis on living A431 cells incubated with 0.05 nM AF488-conjugated MinE07. Results are consistent with those shown on Fig. 2a, obtained using same aptamer, and concentrations, but conjugated to Atto647N.

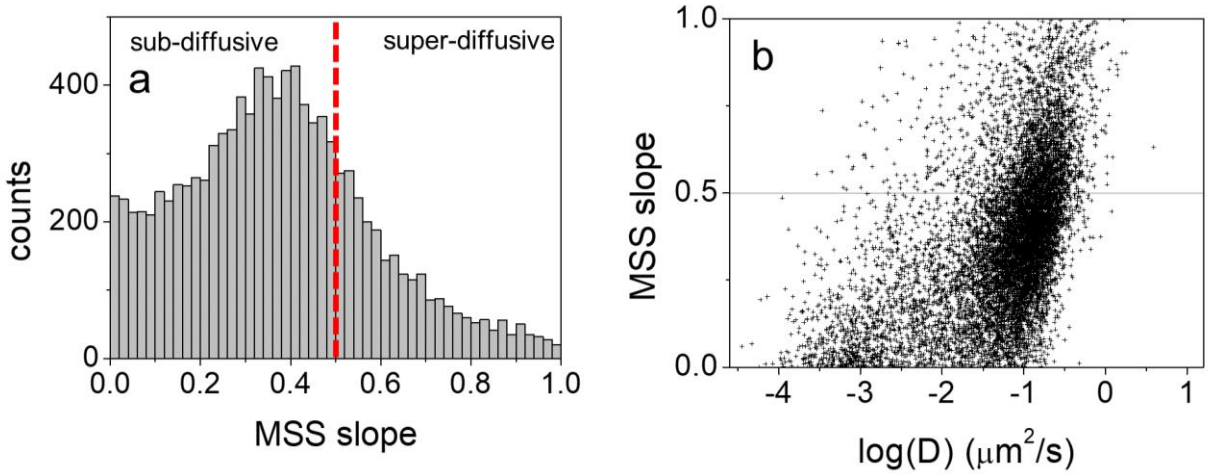

Figure S2. EGFR diffusive behavior obtained from single-molecule tracking analysis on A431 cells incubated with Atto647N-conjugated MinE07 (0.05 nM). This diffusive status corresponds to the data shown in Fig. 2a-c. (**a**) The slope obtained from the moment scaling spectra analysis (MSS slope) for each trajectory is reported. (**b**) A scatter plot of the diffusion coefficients (D) and corresponding MSS slope calculated by tracking analysis are shown. For a free (Brownian) bi-dimensional diffusion, the expected MSS slope value is 0.5, while 0 indicates a stationary molecule and 1 indicates uniform and directed motion. Therefore, sub-diffusive or confined diffusion (0 < MSS slope < 0.5) and super-diffusive or directed diffusion (0.5 < MSS slope <1) can be discriminated.

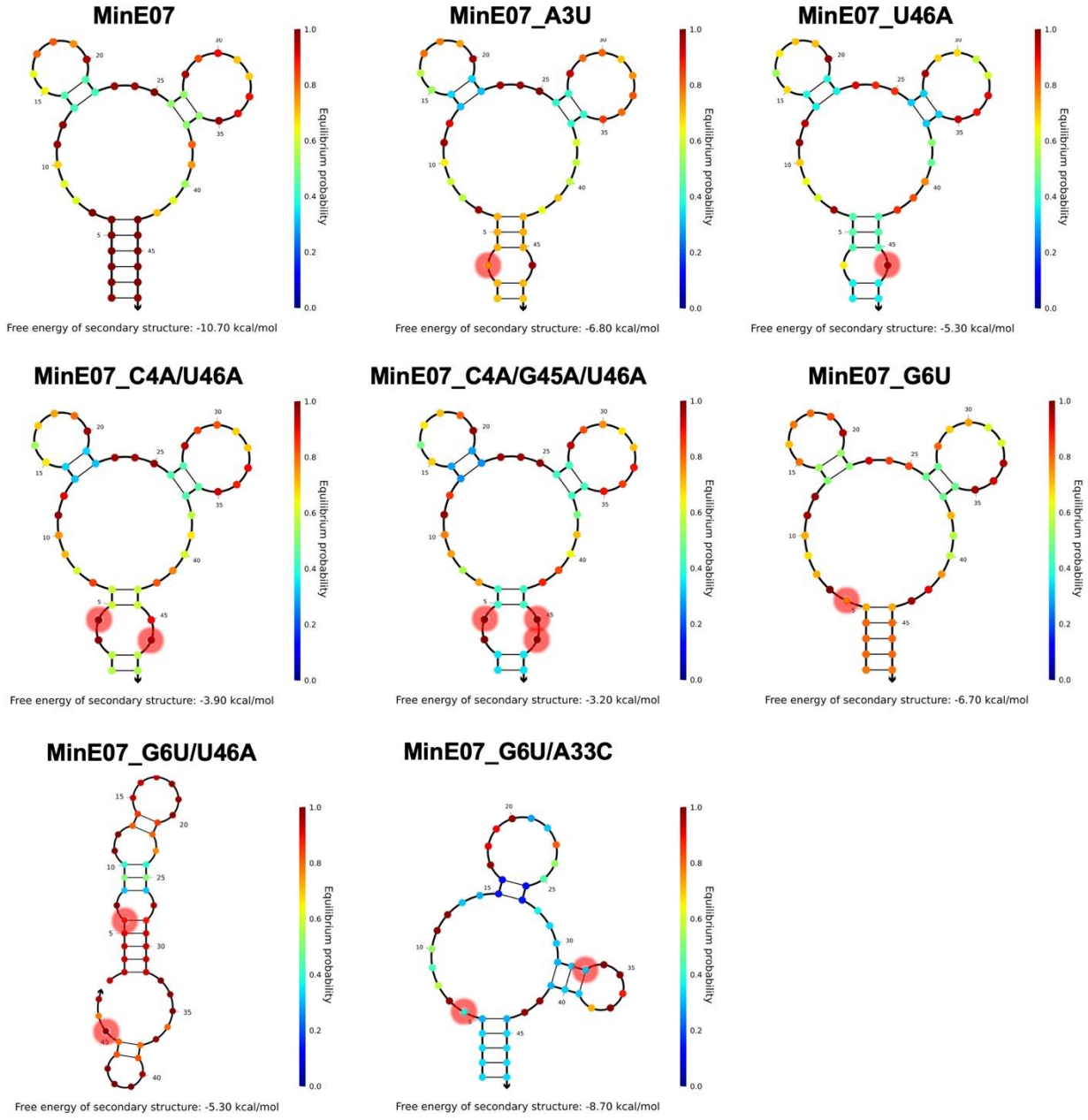

Figure S3. Minimum free energy (MFE) secondary structures of MinE07 and all tested variants predicted by NUPACK software[4]. All aptamer sequences are listed in Table S2. All default NUPACK parameters were used except the energy settings. As energy parameters, we exploited the sets reported by Mathews et al., J Mol Biol 1999. For each aptamer sequence, the predicted formation (*i.e.*, equilibrium probability) for internal domains with duplex or single-stranded regions based on NUPACK calculations is reported on the right. Point mutations within MFE structure of each MinE07 variant are highlighted in red. Values of Gibbs free energy (ΔG, kcal/mole) calculated by NUPACK were reduced in all variants compared to the parental aptamer. MFE structures of five variants (MinE07_A3U; MinE07_U46A; MinE07_C4A/U46A; MinE07_C4A/G45A/U46A; MinE07_C4A/G45A/U46A; MinE07_G6U) were predicted to be similar to the one showed by MinE07, albeit ΔG values were lower. Only two variants (MinE07_G6U/U46A and MinE07_G6U/A33C) displayed a different MFE structure. Mfold[5] was also used to predict secondary structures of these two variants (MinE07_G6U/U46A and MinE07_G6U/A33C) using constrains to resemble the folding of the parental sequence (*i.e.*, forcing a string of base pairs). However, predicted MFE structures and calculated ΔG values for the two variants did not resemble the MinE07 conformation, but instead were identical to the MFE structure of MinE07_G6U (data not shown). G6U is a key point mutation that was found in all three variants that displayed lower affinity than the parental sequence (see Fig. S4). This suggests that such mutation is indeed required to favor presence of alternative conformers of MinE07 with less favorable binding properties to EGFR.

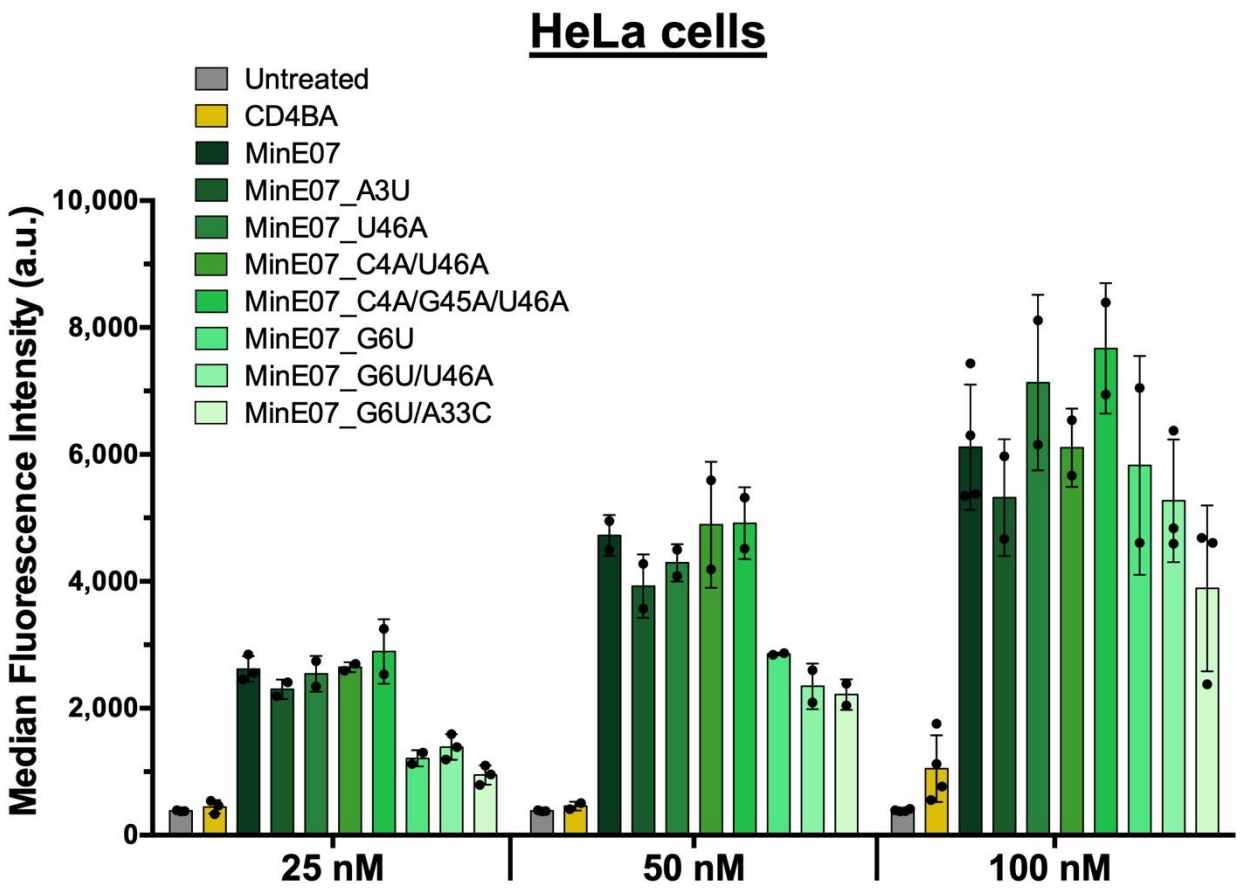

Figure S4. Cell binding properties of Cy5-conjugated aptamer probes. A 2-fold molar excess of anti-EGFR aptamers (MinE07 and its variants) and a control aptamer sequence (CD4BA) were annealed with increasing concentrations of Cy5-anti-tail (25, 50, 100 nM) and their abilities to bind EGFR-overexpressed HeLa cells were assessed by flow cytometry after 1h incubation at 37°C in DPBS containing 5 mM $MgCl_2$. Four variants (MinE07_A3U; MinE07_U46A; MinE07_C4A/U46A; MinE07_C4A/G45A/U46A; MinE07_C4A/G45A/U46A) displayed similar aptamer-mediated cell staining to the one showed by MinE07. In contrast, three variants (MinE07_G6U, MinE07_G6U/U46A and MinE07_G6U/A33C) showed reduced binding of HeLa cells. Results are based on a minimum of two independent experiments.

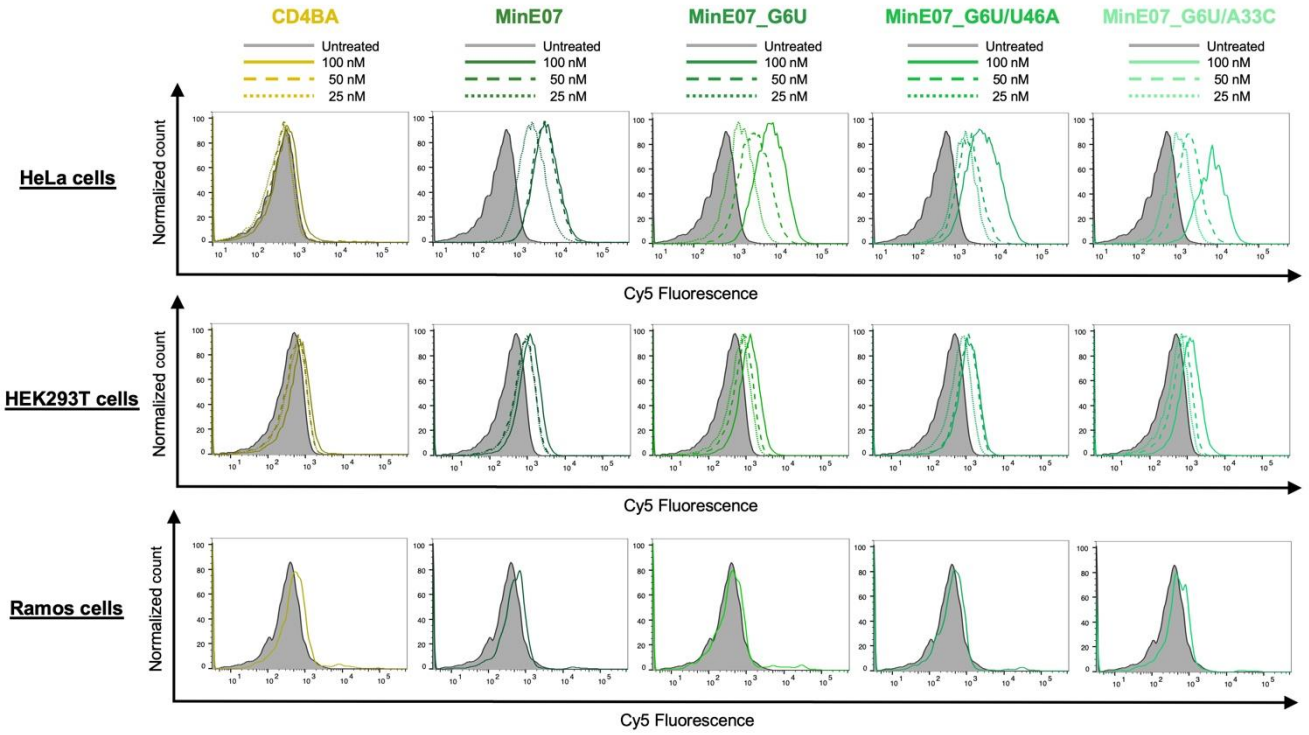

Figure S5. Cell binding properties of Cy5-conjugated anti-EGFR aptamer probes in cell lines with differential expression of EGFR: overexpression (HeLa cells), low expression (HEK293T cells), and no expression (Ramos cells). A 2-fold molar excess of anti-EGFR aptamers (MinE07 and its three variants) and a control aptamer sequence (CD4BA) were annealed with increasing concentrations of Cy5-anti-tail (25, 50, 100 nM). Their abilities to bind HeLa, HEK293T, and Ramos cell lines were assessed by flow cytometry after 1h incubation at 37°C in DPBS containing 5 mM $MgCl_2$. MinE07 and its three variants (MinE07_G6U, MinE07_G6U/U46A and MinE07_G6U/A33C) showed differential binding of these three cell lines that is dependent on the reported surface levels of EGFR. Since aptamer binding of Ramos cells upon incubation with the highest concentration of probes (100 nM) did not show any significant binding, the lowest concentrations (25 and 50 nM) were not tested. Representative flow cytometry curves for 25, 50 and 100 nM are shown as dotted lines, as dashed lines, and as solid lines, respectively. Grey filled curves: untreated cells. Normalized cell count is reported on the *y*-axis, while on the *x*-axis is shown a log scale of Cy5 fluorescence intensity. All curves are representative of at least two independent experiments. Complete results are shown as bar charts in Fig. S6.

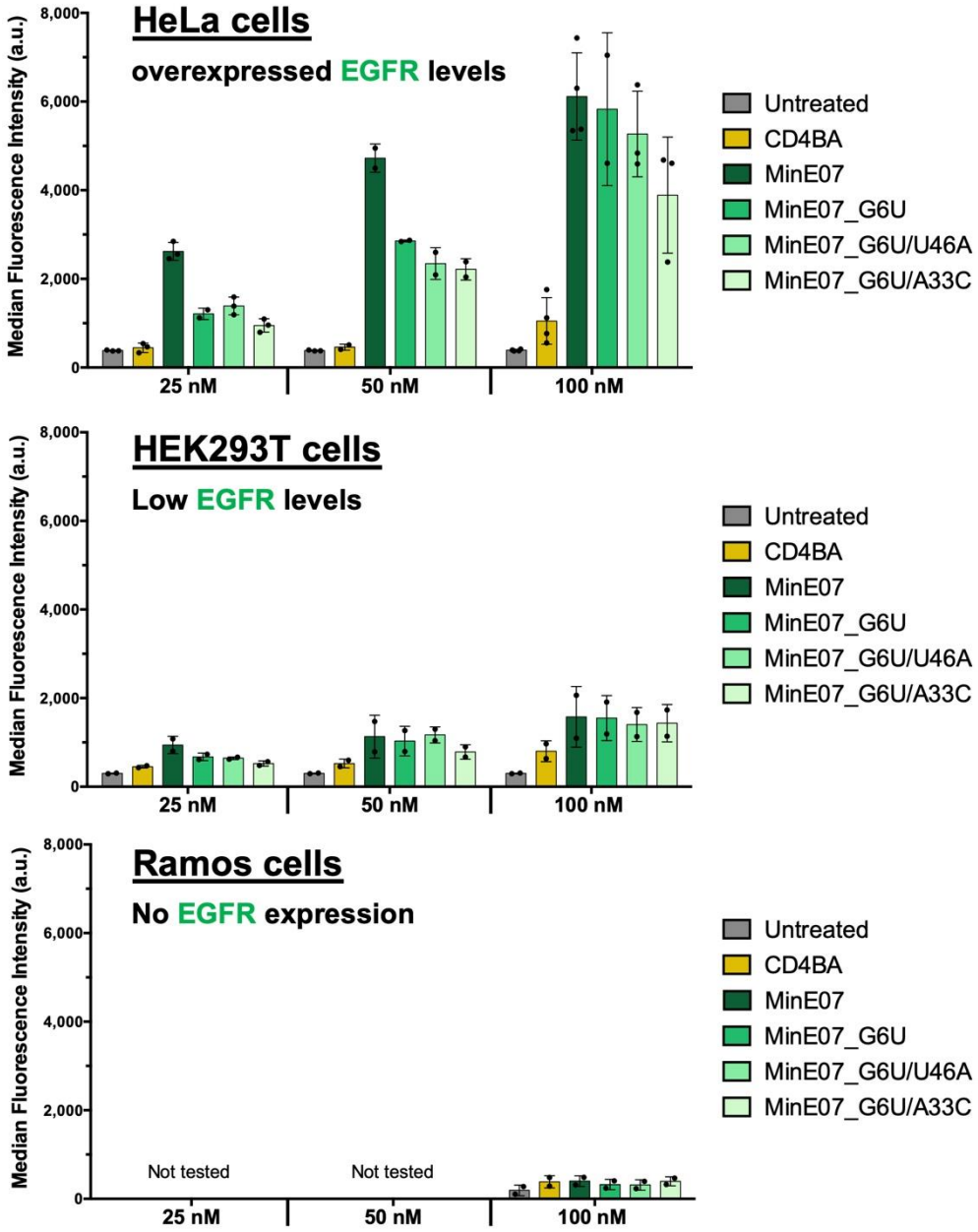

Figure S6. Cell binding properties of Cy5-conjugated anti-EGFR aptamer probes in cell lines with differential expression of EGFR: overexpression (HeLa cells), low expression (HEK293T cells), and no expression (Ramos cells). A 2-fold molar excess of anti-EGFR aptamers (MinE07 and its three variants) and a control aptamer sequence (CD4BA) were annealed with increasing concentrations of Cy5-anti-tail (25, 50, 100 nM) and their abilities to bind HeLa, HEK293T, and Ramos cell lines were assessed by flow cytometry after 1h incubation at 37°C in DPBS containing 5 mM $MgCl_2$. MinE07 and its three variants (MinE07_G6U, MinE07_G6U/U46A and MinE07_G6U/A33C) showed differential binding of these three cell lines that is dependent on the surface levels of EGFR. Values of median fluorescence intensity (MFI) are reported on the *y*-axis, while on the *x*-axis is shown the aptamer concentration tested. Flow cytometry results are based on a minimum of two independent experiments.

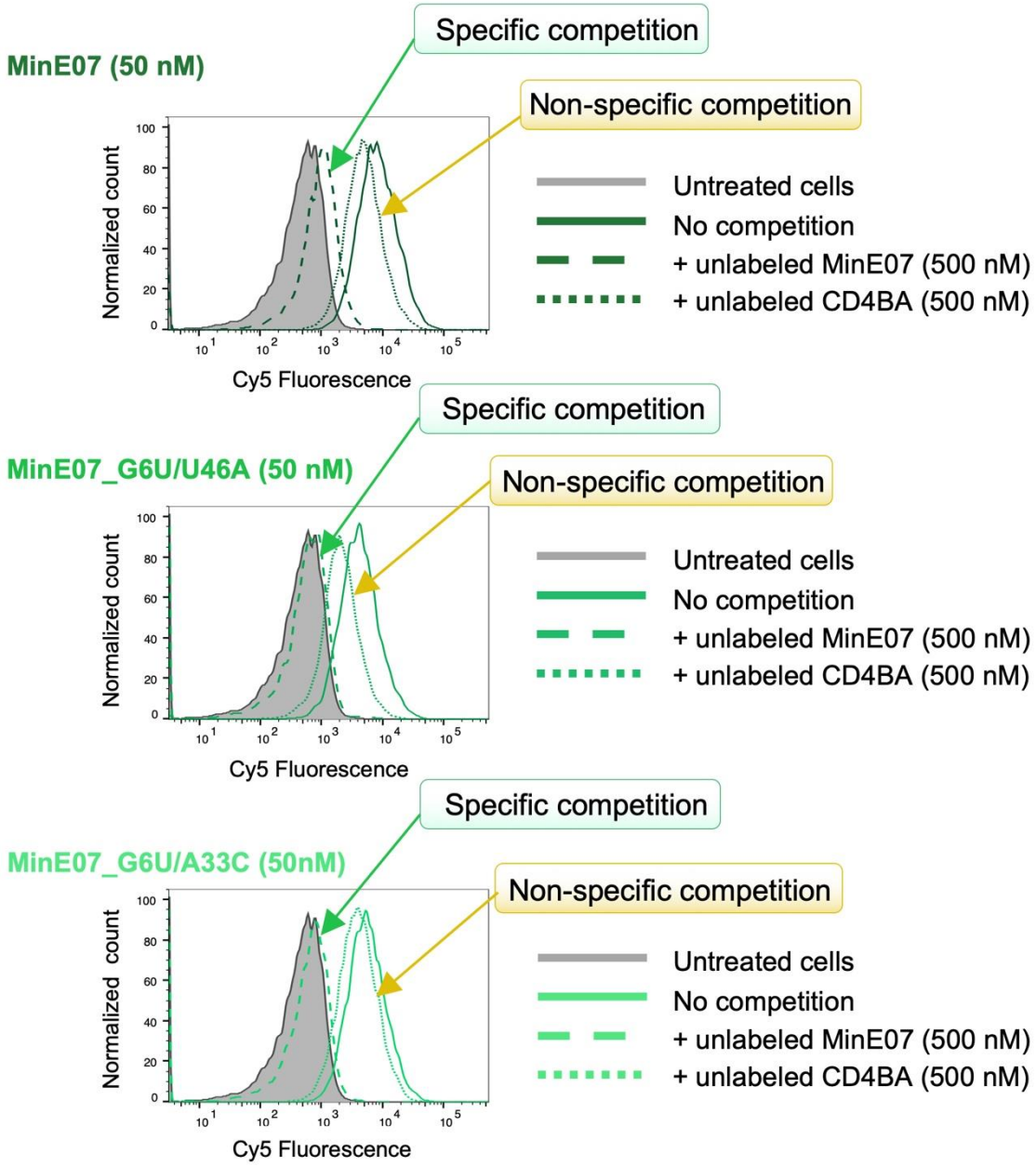

Figure S7. Competition binding assays were performed on HeLa cells. A 2-fold molar excess of anti-EGFR aptamers (MinE07 and two variants) were annealed with 50 nM Cy5-anti-tail and their abilities to bind HeLa cells were tested in absence of competitors (solid lines), in presence of 10-fold molar excess of specific competitor, *i.e.*, MinE07 (dashed lines), or non-specific competitor, *i.e.*, CD4BA (dashed lines). Binding of HeLa cells was tested by flow cytometry after 1h incubation at 37°C in DPBS containing 5 mM $MgCl_2$. Cell staining due to the anti-EGFR aptamers (MinE07, MinE07_G6U/U46A, and MinE07_G6U/A33C) was drastically reduced when they were co-incubated with 10-fold molar excess of specific competitor. In contrast, only a minor reduction of cell staining was observed upon incubation with the non-specific competitor. Grey filled curves: untreated cells. Normalized cell count is reported on the y-axis, while on the x-axis is shown a log scale of Cy5 fluorescence intensity. All flow cytometry curves are representative of two independent experiments.

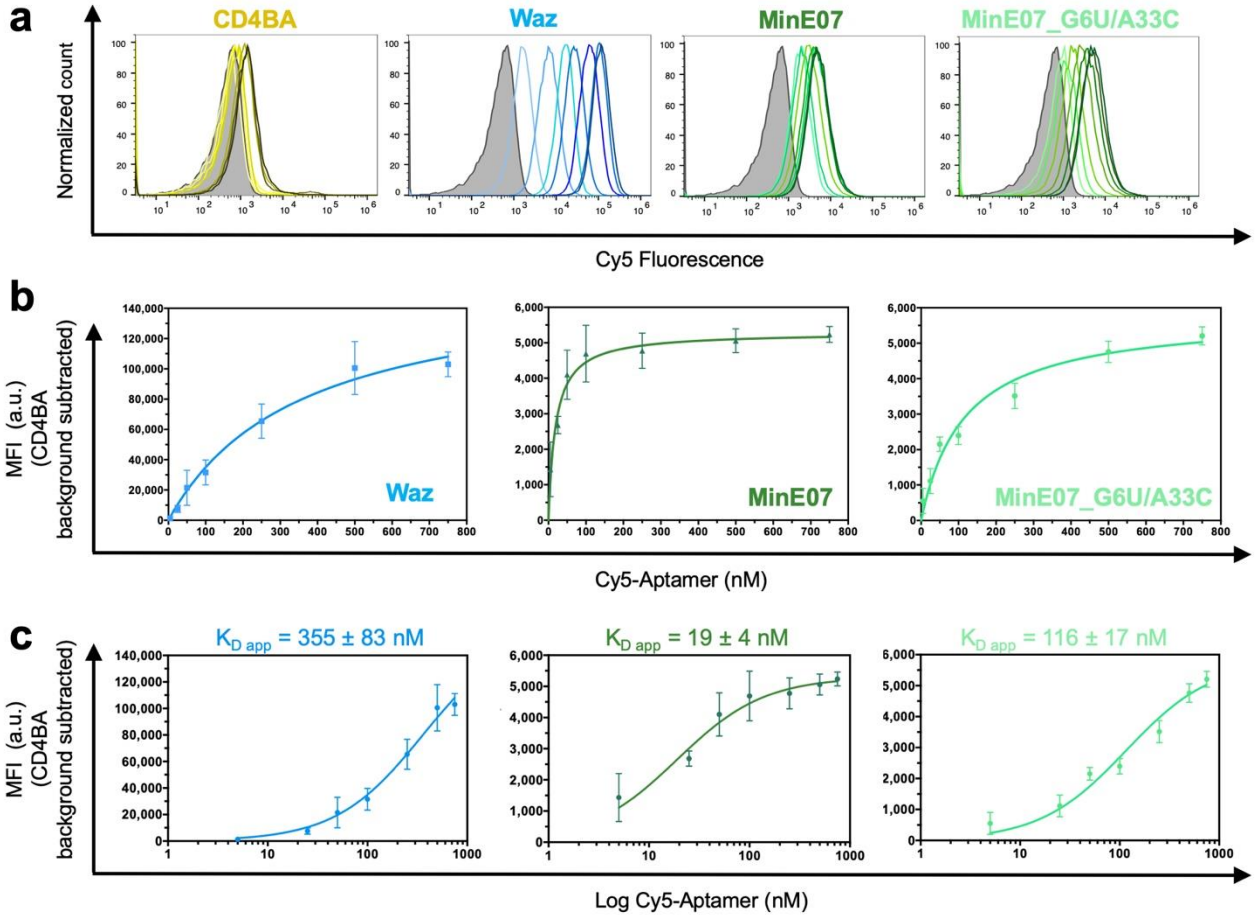

Figure S8. (**a**) Representative flow cytometry curves of titration experiments. A 2-fold molar excess of Waz (blue), MinE07 (dark green), and MinE07_G6U/A33C (light green) and a control CD4BA (gold) were annealed with increasing concentrations of Cy5-anti-tail (5, 25, 50, 100, 250, 500, 750 nM) and their abilities to bind HeLa cells were assessed by flow cytometry after 1h incubation at 37°C in DPBS containing 5 mM $MgCl_2$. For all samples, increased magnitude of cell staining was observed in a dose-dependent manner. A gradient of color was used for each aptamer sample to indicate the different levels of cell staining, where the darkest shade corresponds to the highest cell staining (at 750 nM). Normalized cell count is reported on the *y*-axis, while on the *x*-axis is shown a log scale of Cy5 fluorescence intensity. All flow cytometry curves are representative of three independent experiments. (**b**) Plots of median fluorescence intensity (MFI) after subtraction of non-specific binding (CD4BA contribution) versus aptamer concentration are shown for Waz, MinE07, and MinE07_G6U/A33C. (**c**) Plots of median fluorescence intensity (MFI) after background subtraction versus log scale of Cy5-aptamer concentration are shown. Apparent K_D values were calculated after background subtraction (see materials and methods). Results are based on a minimum of three independent experiments. Importantly, apparent K_D values measured for Waz aptamer (355 ± 83) nM and MinE07 are in agreement with previous estimates from flow cytometry (see Ref. 30 and 31 in main text)

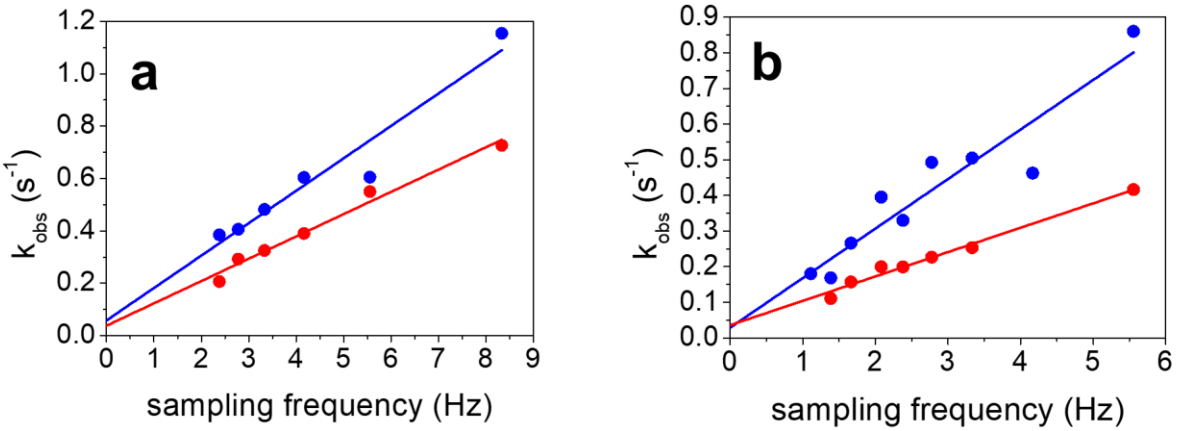

dye	sampling	k_{bl} (s^{-1})	k_{off} (s^{-1})
AF488	2-9 Hz	2.06	0.058
	1-6 Hz	2.32	0.029
Atto647N	2-9 Hz	1.42	0.038
	1-6 Hz	1.17	0.036

Figure S9. Observed dissociation rate (k_{obs}) obtained from single-molecule trajectories duration on A431 cells exposed to low-affinity MinE07 aptamer conjugated to AF488 (blue) or Atto647N (red) at increasing sampling frequency. Discontinuous illumination was employed to modulate the sampling frequency while keeping a constant exposure time in each cycle. Measurements were repeated using a faster (a) and a slower (b) range of sampling frequencies. The results of the fitting with a linear model are shown, where slope is proportional to photo-bleaching rate (k_{bl}) while the intercept corresponds to the dissociation rate (k_{off}) of the aptamer-EGFR complex. Values calculated from fitting are reported in the table.

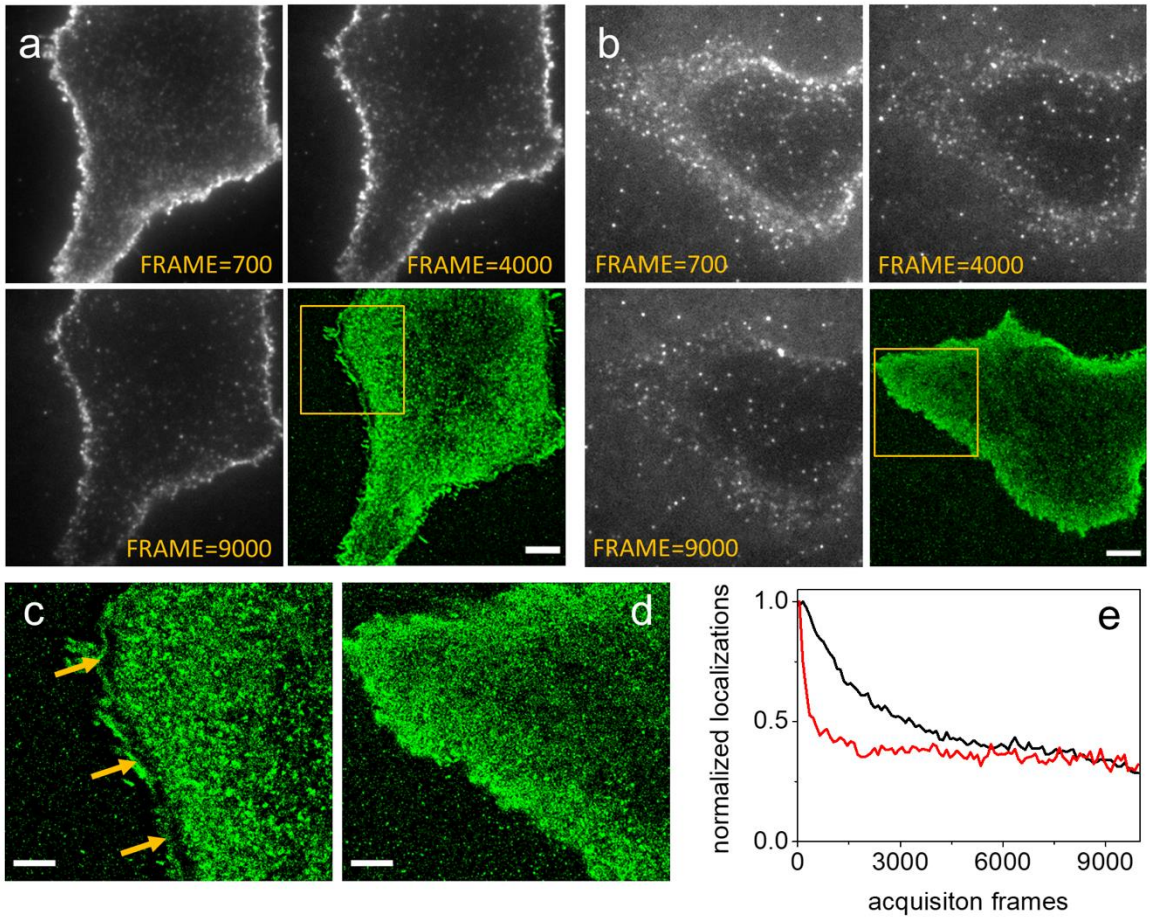

Figure S10. (**a-b**) Comparison of different acquisition frames and final reconstructed PAINT images for A431 cells incubated with 3 nM high-affinity MinE07 (**a**) or low-affinity MinE07 (**b**) conjugated to Atto647N. Scale bars 5 µm. Differences between the two probes can be appreciated by a comparison of the acquisition frames in the two panels (a-b). Panel **b** shows that stable imaging conditions are quickly reached after frame 700, where single-molecules are easily localized. In contrast, panel **a** shows significant initial probe overloading at the cell edges, where single-molecule positions are hardly localized, which is followed by continuous and slow photo-bleaching through the whole acquisition. (**c-d**): Close ups of PAINT images on basolateral membrane obtained with high-affinity MinE07 (**c**) and low-affinity MinE07 (**d**), corresponding to the yellow squares in panels **a** and **b**, respectively. Scale bars 2 µm. Artifacts due to overloading with fluorescent probes are indicated with arrows. (**e**) comparison of localizations rate during acquisition for high-affinity MinE07 (black) and low-affinity MinE07 (red) conjugated to Atto647N. While for high-affinity MinE07 the number of localizations decreases during the whole acquisition (black curve), a constant localization rate is achieved for low-affinity MinE07, after a fast initial decrease (red curve). The overloading of A431 edges and the unsteady localization rate observed for high-affinity MinE07 probe are equally observed under increased and reduced irradiation intensities, demonstrating that these issues are related to the inherent affinity of the probe rather than the specific choice of acquisition parameters.

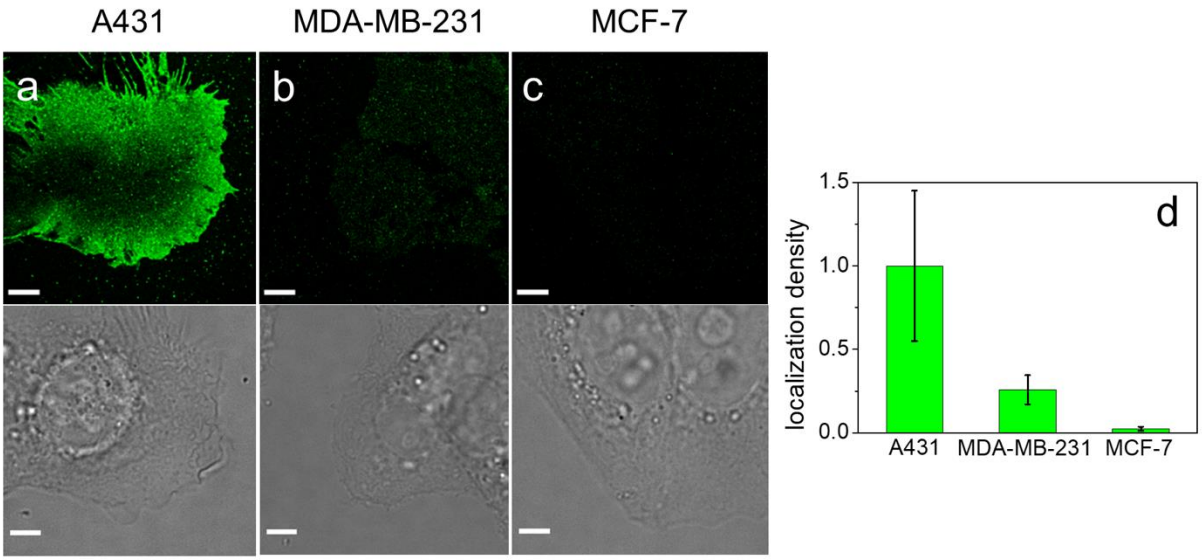

Figure S11. Representative STORM images after EGFR immunostaining (top images) and corresponding bright field images (bottom images) of fixed A431 (**a**), MDA-MB-231 (**b**), and MCF-7 (**c**) cells. Scale bars 5 µm. (**d**) Comparison of the localization density calculated from STORM images in an area corresponding to cell basal membrane is reported. Values were normalized to localization density on A431 cells.

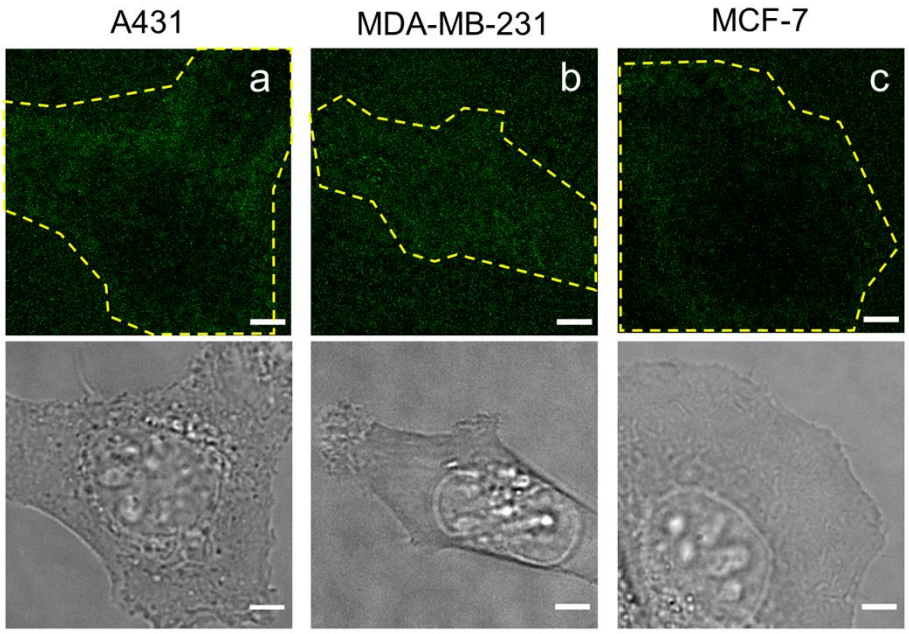

Figure S12. (**a-c**): Representative bright field images (bottom) and reconstructed PAINT images (top) obtained upon incubation of living A431 (**a**), MDA-MB-231 (**b**) or MCF-7 (**c**) cells with the non-targeting control Atto647N-conjugated CD4BA aptamer (7 nM). Yellow dashed lines are intended as a visual aid to identify cell outlines in the PAINT images. Scale bars 5 µm.

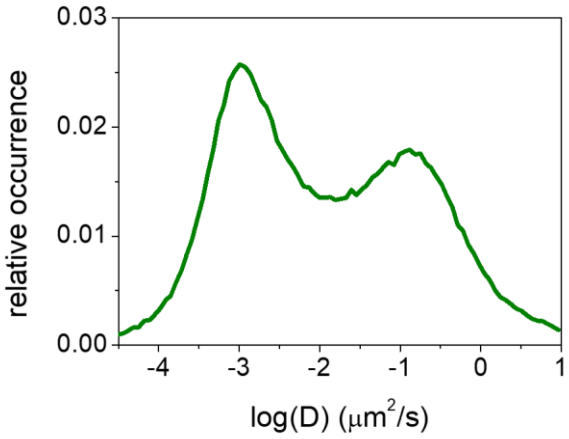

Figure S13. Distribution of the measured diffusion coefficient values upon incubation of living MDA-MB-231 cells with Atto647N-conjugated low-affinity MinE07 (17 nM).

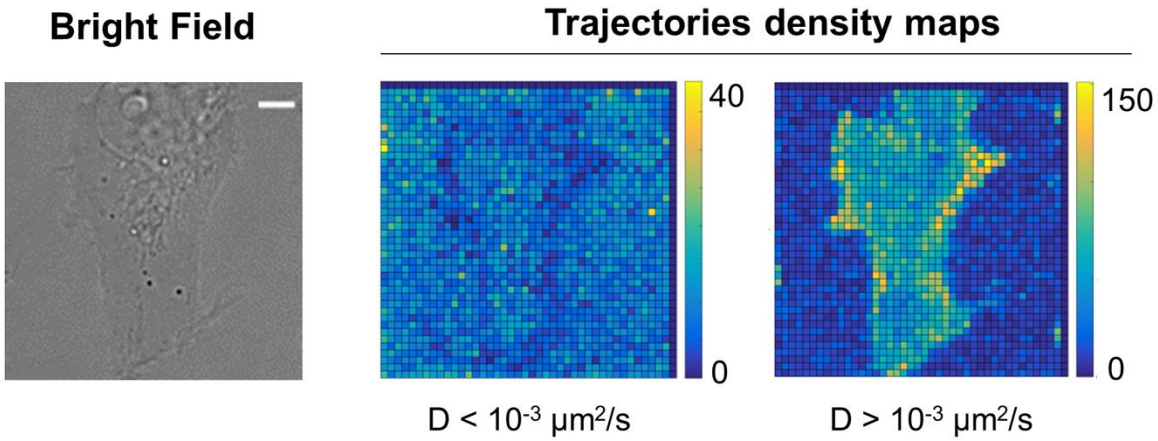

Figure S14. Maps of trajectory densities on a representative MDA-MB-231 cell incubated with Atto647N-conjugated low-affinity MinE07 (17 nM). Maps are reconstructed considering detected trajectories longer than 5 frames and applying a filtering process that selects trajectories with a D value lower than 10^{-3} µm^2/s (static) or higher than 10^{-3} µm^2/s. Colors indicate the number of selected trajectories centered within each pixel of the map (size 1 µm). The exact color-scale is reported on the bar on the right of each image. A bright field image of the same cell is provided as reference (scale bar 5 µm). Static trajectories are equally distributed between cell membrane and glass coverslip area, while non-static trajectories are mainly located on the cell membrane area.

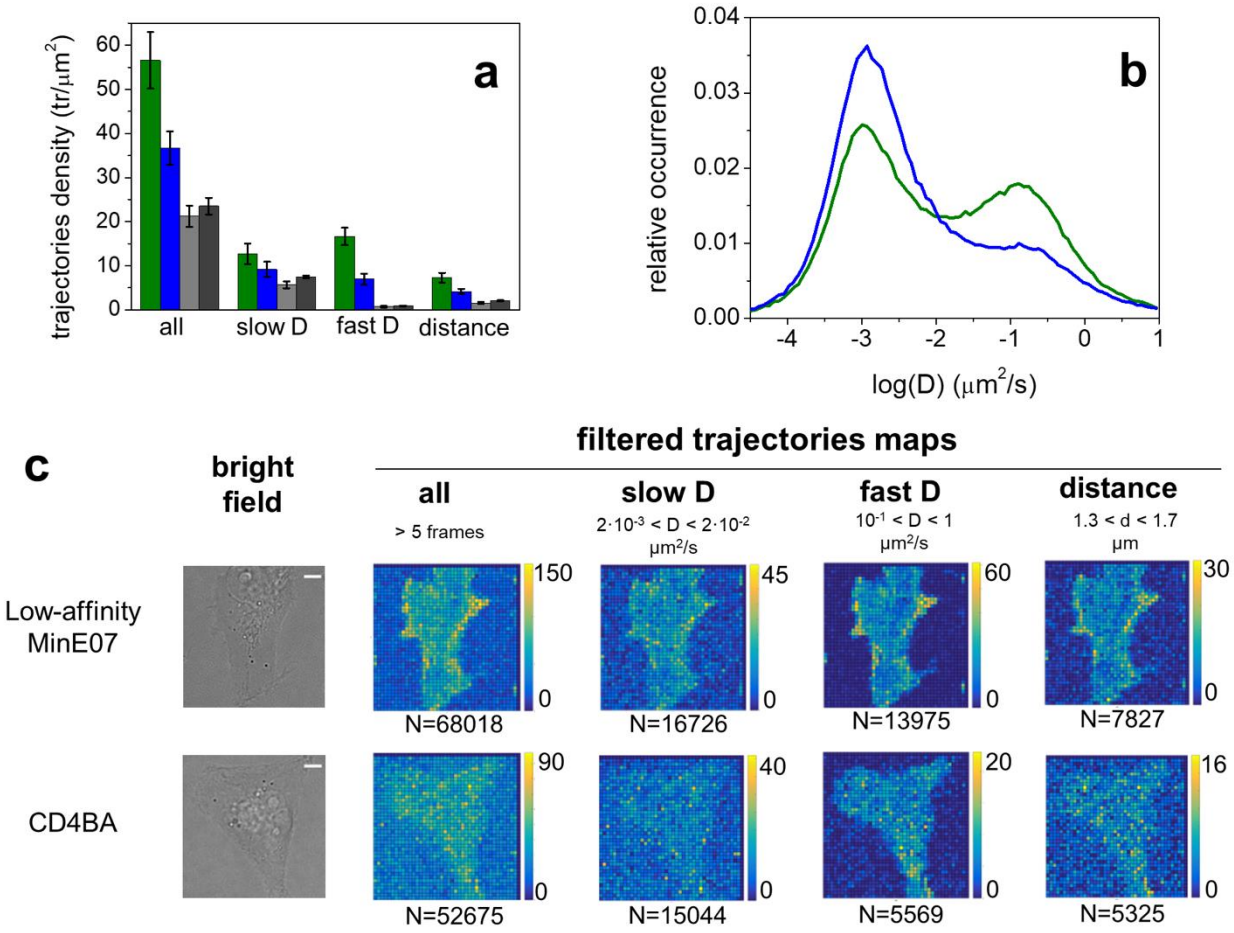

Figure S15. (**a**) Comparison of trajectory densities on the cell membrane area after several applied filters, obtained upon incubation of living MDA-MB-231 cells with 17 nM of Atto647N-conjugated low-affinity MinE07 (green) or CD4BA (blue) probes (5 cells, mean ± st. dev.). Densities on a coverslip surface area are also reported for both low-affinity MinE07 (light grey) and CD4BA (dark grey) probes. (**b**) Diffusion coefficient distributions from all trajectories obtained with low-affinity MinE07 (green, N=312293, 5 cells) and CD4BA (blue, N=243862, 5 cells). A significant difference between the two distributions is readily observed, with a majority of immobile molecules observed for CD4BA probe in comparison to low-affinity MinE07. (**c**) Maps of trajectory densities obtained on two representative MDA-MB-231 cells incubated with 17 nM low-affinity MinE07 (top) or CD4BA (bottom). Maps are reconstructed considering all detected trajectories (all), or after applying different filters. Colors indicate the number of selected trajectories centered within each pixel of the map (size 1 μm). The color-scale is reported on the bar on the right of each image, while the total number of selected trajectories is at the bottom. A bright field image of the same cell is provided as reference (on the left). Density values obtained with CD4BA probe are systematically lower than those of low-affinity MinE07. Additionally, distribution of trajectories provided by the maps is also different for the two probes.

SUPPORTING INFORMATION

Supplementary Videos

Video S1:
A431 cell exposed to 0.05 nM of MinE07 aptamer conjugated to Atto647N. Sampling time 240 ms, Scale bar 5 µm.

Video S2:
A431 cell simultaneously exposed to Atto647N-conjugated MinE07 aptamer (0.05 nM, green) and AF488-conjugated WAZ aptamer (0.20 nM, magenta). Sampling time 120 ms, Scale bar 5 µm.

Supplementary Notes

Effect of non-specific interactions on single-molecule tracking data

Our aptamer-based approach for SMT of EGFR (Fig. 2) exploits diffusing, non-invasive probes rather than genetically encoded fluorescent tags. Therefore, it is important to monitor potential contributions of non-specific interactions, such as adsorption of probes onto the glass coverslips, binding of non-target, surface-exposed molecules, or dye-driven interactions with membrane lipid bilayer. To this end, SMT experiments were performed using MinE07 aptamer conjugated to a different dye, AlexaFluor488, which photobleaches more rapidly but displays a lower affinity for lipid bilayers than Atto647N[6,7]. Diffusion coefficient distribution and average D values for AlexaFluor488-conjugated (Fig. S1) and Atto647N-conjugated (Fig. 2a) aptamer were very consistent, with only minor variations in the D values, mainly on the immobile population. In addition, we performed SMT analysis using an RNA aptamer that binds selectivity to human CD4[8,9], a membrane protein receptor expressed on the surfaces of normal and cancerous T cells but not on A431 cells and other solid tumor cells. Upon incubation of A431 cells with Atto647N-conjugated CD4-binding aptamer (CD4BA), only a weak fluorescent signal was observed, as a consequence of minimal non-specific interactions (see Fig. S4–S8 and Fig. 4).

Strategies to improve sensitivity of live-cell PAINT: probe concentration and macromolecular crowding agents

Initial localization densities were calculated from PAINT images on three cancer cell lines (A431, MDA-MB-231 and MCF7 cells, as shown in Fig. 4) using 7 nM of ATTO647N-aptamer probes. Signal-to-noise ratio (SNR), defined as the signal due to the anti-EGFR aptamer divided by signal for CD4BA, was measured for each cell line (Fig. 4d). Localization density obtained for A431 cells, characterized by high EGFR overexpression, using low-affinity MinE07 (7 nM) was ~2.9-fold higher than that obtained with the same concentration of CD4BA, which in turn displayed equivalent signal to the coverslip surface. Variability in the localization density for low-affinity MinE07 on A431 cells (Fig. 4d) was likely associated with the heterogeneity of cell features, such as cell morphology, migration rate or proliferation rate, all of which can change when culturing cells *in vitro*[10] and contribute to heterogeneity within and between samples. In contrast, SNRs of localization densities measured in MDA-MB-231 and MCF-7 cell lines showed little difference between low-affinity MinE07 and CD4BA or the coverslip surface using 7 nM as probe concentration (Figs. 4d and SN1), consistent with a reduced expression of EGFR in these two cell lines[11,12]. Particularly, localization density displayed by the low-affinity MinE07 anti-EGFR aptamer on MCF-7 cells was statistically equivalent to the control values obtained for CD4BA or the coverslip surface (Fig. 4d). In the case of MDA-MB-231 cell line, localization density for low-affinity MinE07 was slightly above background (*i.e.,* ~1.2-fold higher than CD4BA), with only weak statistical significance (Figs. 4d and SN1). As expected, these results illustrate that SNR was strongly affected by the amount of target receptors expressed on the cell surface. Using these labeling conditions, a high SNR (~2.9) was found only when cells expressed especially high levels of EGFR (as in the case of A431 cells).

"Surface passivation" is commonly used in single-molecule TIRF imaging to minimize interactions between probes and coverslip surfaces, thus increasing SNR. However, cationic polymers commonly used in this process, such as poly-L-lysine-grafted polyethylene glycol (PLL-PEG)[13], are likely to form electrostatic complexes with aptamers that disrupt their 3D structures and target binding. Therefore, we investigated whether other changes in labeling conditions could improve SNR even on breast cancer cell lines with moderate and low EGFR levels.

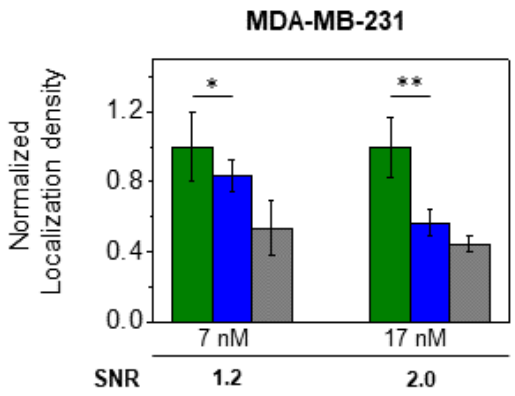

Figure SN1. Normalized localization densities on the membrane of MDA-MB-231 cells are reported using two concentrations of Atto647N-conjugated aptamer probes (7 and 17 nM). Green and blue bars report values obtained with low-affinity MinE07 and CD4BA apatmers, respectively. Grey bars reports values obtained on the glass coverslip surface. Means and standard deviations are reported in histograms. Statistical analysis was performed with non-parametric Mann-Whitney test: **: $p < 0.05$; *: $p < 0.1$;

Thus, we increased the concentration of aptamer probe to 17 nM and imaged EGFR on both MDA-MB-231 and MCF-7 cell lines. Localization density with improved SNR was observed in MDA-MB-231 cells under these conditions. Values of EGFR density labeled with low-affinity MinE07 was ~2-fold and ~2.5-fold higher, respectively, than CD4BA and coverslip surface (Fig. SN1). Both values were more similar to those measured in A431 cell line. To validate that this result was not cell line dependent, two additional cell lines (HeLa and A549 cells) with similar reported expression levels[14–16] as for MDA-MB-231 cells (Table S1) were incubated with 20 nM of aptamer probes (Fig. SN2). Similar values of relatively high SNR (~2-fold) were observed even in HeLa cells (Fig. SN2a,d), for which the reported EGFR expression is the lowest among these cell lines[15,16] (Table S1). In contrast, using higher concentrations of aptamer probe (17 nM) did not result in a significant difference between low-affinity MinE07 and CD4BA for MCF-7 cells, for which the EGFR expression level remained below the threshold of detection. Besides the modulation of probe concentration, additional strategies can further improve SNRs. Taking HeLa and A549 as model for cells with moderate EGFR expression, we aimed to address whether non-invasive changes in the labeling conditions, obtained by introducing additional non-specific competitors, could increase the overall SNR ratio of the measurements.

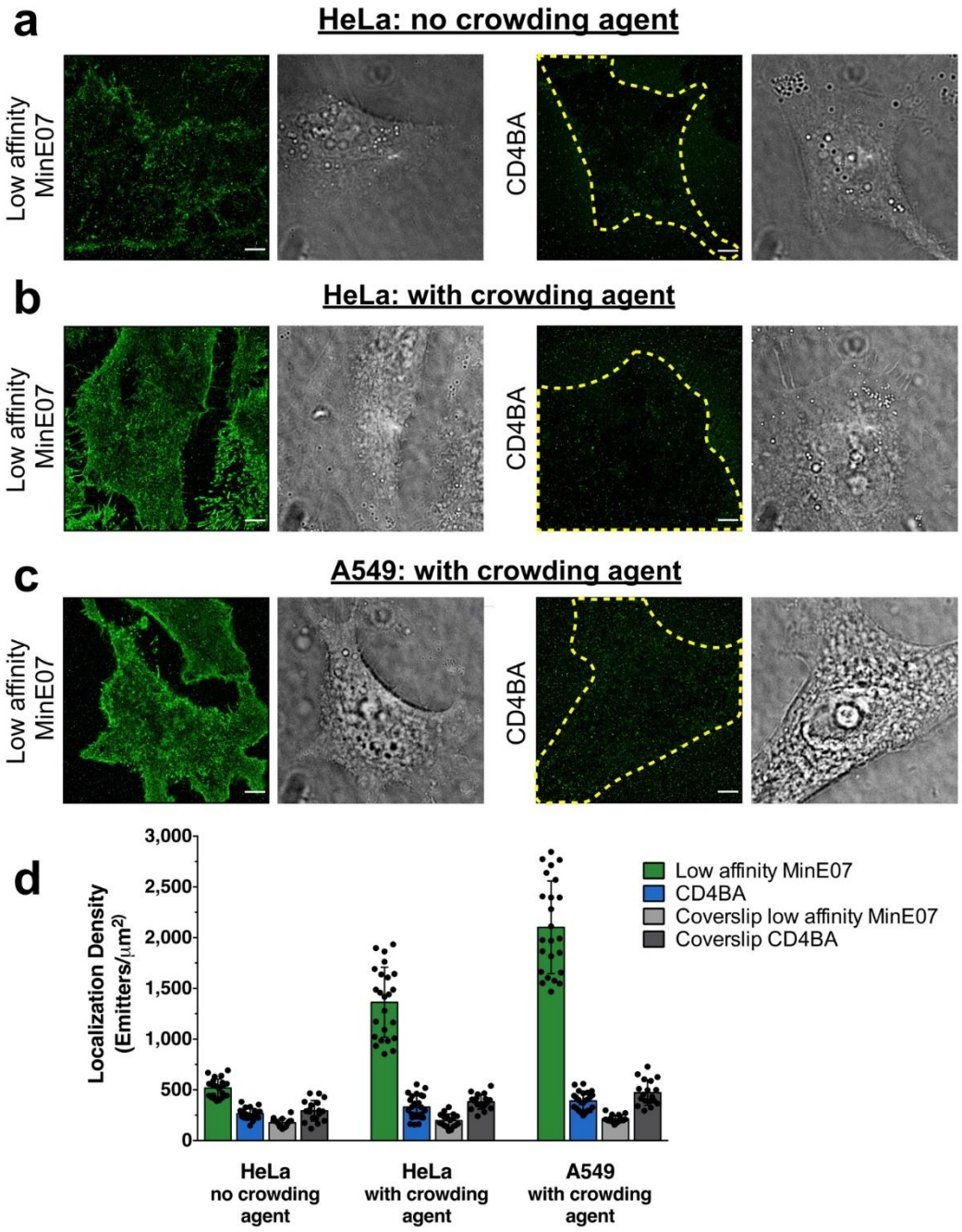

Figure SN2. (**a-c**) Reconstructed live-cell PAINT images and corresponding bright field images obtained upon incubation of living HeLa or A549 cells with Atto647N-conjugated aptamer samples (20 nM). Yellow dashed lines are intended as a visual aid to identify cell outlines in the PAINT images obtained with CD4BA aptamer. Scale bar 5 μm. (**d**) Localization density (Emitters/μm2) was measured for each sample as follows. In areas with cells (green and blue bars for low-affinity MinE07 and CD4BA, respectively), four Regions of Interest (ROIs) were measured in each of three different fields of view for two independent experiments (total 24 ROIs).

A similar approach was used to assess interactions of fluorescent aptamers on the glass coverslip by sampling localization density in areas with no cells (total 18 ROIs) (light grey and dark grey bars for low-affinity MinE07 and CD4BA, respectively). ThunderSTORM plugin for ImageJ[17] were used to reconstruct PAINT images on HeLa and A549 cells using the following parameters. Briefly, camera setup was set as follows: pixel size (99 nm); photoelectron per A/D count 3.6; base level [A/D count] 100; and an EM gain of 300. The following parameters were used to find and fit the signal of each fluorescent emitter: image filtering – Difference-of-Gaussians filter (sigma 1 = 1.2 and sigma 2 = 3.0); approximate localization of molecules – Local maximum (peak intensity threshold: std(Wave.F1), connectivity: 8-neighbourhood); sub-pixel localization of molecules – Integrated Gaussian (fitting radius: 4 px, fitting method: Weighted Least squares, initial sigma: 1.3 px). Results were filtered by sigma values (sigma > 90 & sigma < 250 nm), and duplicates were removed using a value of distance threshold = 10 nm.

In the live-cell PAINT experiments described throughout this work (except in those shown in Fig. SN2b-c), Atto647N-conjugated aptamer samples (7 nM, 17 nM or 20 nM) were co-incubated with 1 mg/ml of sheared salmon sperm DNA (sssDNA) as competitor for non-specific binding sites on the cell surface. However, additional competitors were used for imaging experiments on HeLa cells shown in Fig. SN2. Thus, a “cocktail of polyanionic competitors” was prepared to include: sssDNA (1 mg/ml), Dextran Sulfate (500 kDa, 1 mg/ml), and an arbitrary 2′F-pyrimidine-modified RNA sequence (2 μM) (see Materials and Methods) that does not bind specifically any cell-surface molecules. Instead of following the standard co-incubation protocol, this cocktail of polyanionic competitors was incubated with HeLa cells prior to the addition of the aptamer samples (20 nM), mimicking the blocking step normally used in immunofluorescence staining. Surprisingly, measurements of localization density (Fig. SN2d) that compare results of Fig. SN2a and SN2b showed that interactions of a control aptamer (CD4BA) with the plasma membrane (blue bars) or with the coverslip surface (dark grey bars) did not diminish using a cocktail of polyanionic competitors. Similarly, low-affinity MinE07 interacted with the coverslip surface in the same extent using either one of the two protocols (light grey bars). These results suggest that using additional polyanionic competitors did not further enhance the blocking effect exhibited by sssDNA. Therefore, interactions with non-specific binding sites either on the cell surface or onto the glass coverslip remained similar. However, the cell specific binding due to the low-affinity MinE07 (green bars) was significantly improved (almost 3-fold for HeLa cells and almost 4-fold for A549 cells) in the presence of the cocktail of polyanionic competitors (Fig. SN2d). Dextran Sulfate is a known MacroMolecular Crowding (MMC) agent that is able to increase the thermodynamic activity in biological systems and enhance molecular interactions[18,19]. In our live-cell PAINT experiments is highly possible that the presence of Dextran Sulfate increased the MMC on the extracellular space, enhancing the fraction of the total volume occupied by macromolecules. This in turn could thermodynamically favor association between low-affinity MinE07 and EGFR molecules on the cell surface. At this regard, a computational work based on Brownian dynamics simulations[20] has recently found that the presence of macromolecular crowding agents (*e.g.*, Dextran Sulfate) can reduce mobility of freely-diffusing ligands (*e.g.*, aptamers) located in the extracellular environment, thus initially limiting their access to the cell membrane. However, once the ligands are located in close proximity with the cell membrane, the MMC effect hampers the motion of ligands away from the cell surface, confining them and increasing their local concentration at the surface. This effect ultimately increases the probability that “productive collisions” occur between ligands and their target receptors (*e.g.*, EGFR)[20]. The diffusive search of receptors is thereby effectively confined to the cell surface with a consequent reduction-of-dimensionality kinetics (from 3D in the extracellular space to 2D onto the cell surface) that can further favor ligand-receptor interactions[21].

Notably, MMC agents could also have an impact on the RNA folding of low-affinity MinE07. MMC can indeed alter the equilibrium between folded and unfolded states of biological macromolecules[22,23]. Therefore, it is also possible that in our experiments Dextran Sulfate favored the transition from an unfolded RNA aptamer conformation (unable to bind EGFR) to a folded and more compacted 3D structure[23] that binds EGFR. Further experiments can possibly rule out whether MMC plays a role on increasing ligand-receptor interactions, altering RNA folding equilibrium, or as a combination of both effects.

In the case of aptamer-based PAINT, we can envision that modulation of aptamer probe or Dextran Sulfate concentration can be fine-tuned to regulate binding kinetics of ligand-receptor interactions, thus achieving optimal PAINT imaging.

Aptamers as silent affinity probe to monitor ligand independent activity of EGFR

Besides the small size and the excellent compatibility with live-cell imaging, MinE07 aptamer shows good potential as a “silent affinity probe”, *i.e.*, a probe that does not perturb the receptor state, to study the ligand-independent activity of EGFR. This point is well supported in the article that reports the selection of the parental E07 as a specific EGFR targeting aptamer[24]. In this work it is shown that the aptamer competes for the binding of EGFR with its natural ligand, EGF. However, E07 does not induce any autophosphorylation of EGFR. E07 also binds both monomeric and dimeric states of recombinant EGFR. These evidences indicate that although E07 (and its truncated sequence MinE07) binds the same binding site of EGF on EGFR (or at least the two binding sites have a significant overlap), this aptamer does not induce conformational changes that activate EGFR and that could lead to the autophosphorylation of the EGFR kinase domains. Therefore, MinE07 aptamer has the potential to be exploited as “silent” labels to study the ligand-independent activity of EGFR with minimal interference on the receptor functional state. In order to further support this hypothesis, we carefully inspected some SMT acquisitions obtained on living HeLa cells to detect changes in the EGFR oligomerization states. The formation of short-lived EGFR dimers could be observed, as reported in Fig. SN3. These findings are consistent with previous works (for instance[25]) and strongly suggest that though MinE07 competes with EGF, the aptamer binding does not preclude the formation of EGFR dimers (or oligomers), which in turn retain their inactive conformation (no MinE07-induced EGFR phosphorylation has been reported).

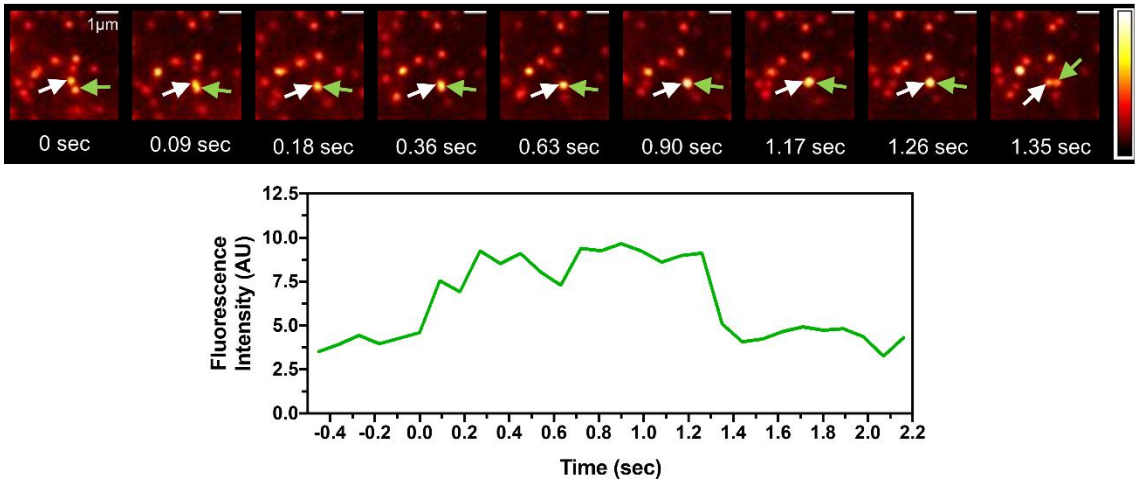

Figure SN3. TOP: example of detection of a short-lived EGFR dimer on living HeLa cells exposed to 20 nM Atto647N-labeled low-affinity MinE07 aptamer. White and green arrows are intended as visual help to identify the emission of the two receptors. BOTTOM: fluorescence intensity time-trace for the fluorescent spot indicated by the green arrow. A nearly 2-fold increase of intensity is observed in the central between 0.0 and 1.4 s, consistently with a transient dimerization.

Similar "close proximity" events, possibly related to the presence of mesoscale domains enriched with EGFR, can be also observed with a two-color approach, as in the Fig. SN4, obtained by simultaneously exposing living A431 cells to low-affinity MinE07 aptamer conjugated with Atto647N (red) and AlexaFluor488 (blue)

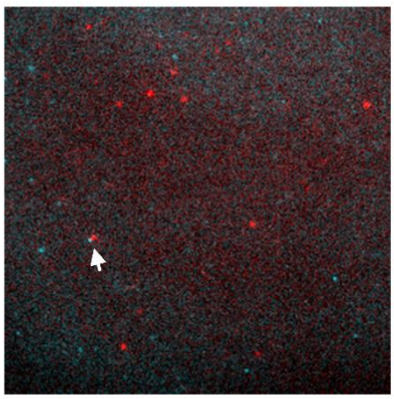

Figure SN4. Representative acquisition frame obtained on a A431 cell simultaneously exposed to Atto647N-conjugated (red) and AlexaFluor488-conjugated low-affinity MinE07 aptamer at sub-nM concentration. The white arrow points a region were two receptors are found in close spatial proximity in two consecutive frames obtained with 647 and 488 channels.

An additional characterization was obtained by analyzing the first acquisition frame obtained on living HeLa cells exposed to high-affinity MinE07. The analysis of a single frame is intended as a "snapshot" in which approximately 1600 diffraction-limited emitters were localized (Fig SN5). Several high-intensity single spots or spots located in close proximity (< 100 nm) are detected, in agreement with the presence of EGFR in oligomers or in close spatial proximity. Following a previous analysis method in which the intensity of single spots was employed to study dimerization of EGF-labelled EGFR [26], we observed that single-spot intensity distributions could be well-fitted with two- or three-Gaussian model (Fig. SN5). Remarkably, the centers of the first two Gaussian differ by a factor ~2, which is consistent with the presence of a dimeric population.

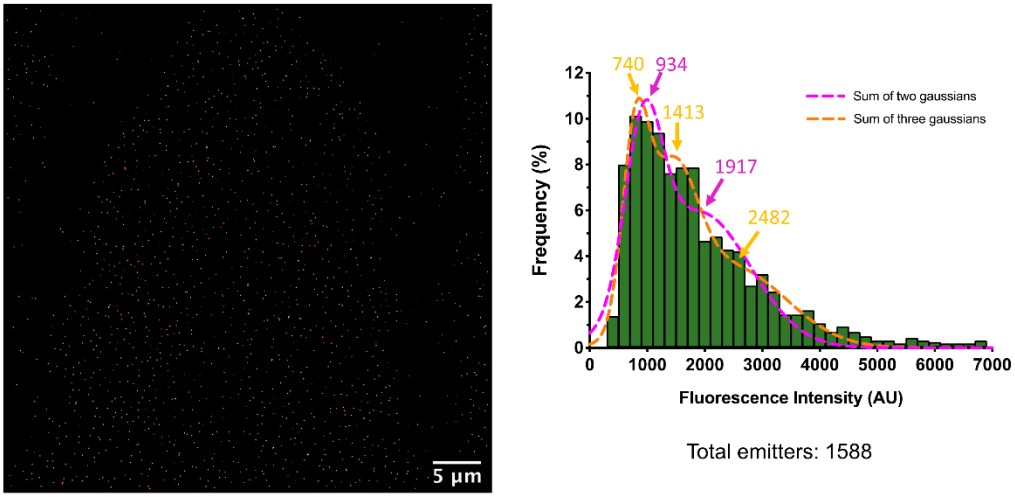

Figure SN5. Example of one live-cell acquisition frame obtained on HeLa cells exposed to 20 nM Atto647N-labeled high-affinity MinE07 (LEFT). 1588 fluorescent spots are detected and their fluorescence intensity distribution (RIGHT) was well-fitted with a 2-Gaussian (magenta) and a 3-Gaussian (orange) model. Center values of the Gaussian curves obtained by the fitting are indicated. Notably, the center-values differ approximately by a factor 2 for both models, consistently with the presence of dimers, i.e. fluorescent spots with doubled intensity.

These preliminary findings highlight how these aptamer probes (both high and low-affinity MinE07) have the potential to monitor the ligand-independent activity of EGFR. High- and low-affinity MinE07 aptamers therefore could represent as valid and complementary alternatives to EGF or other EGFR-activating ligands to study the basal EGFR behavior with single-molecule sensitivity in different biological contexts.

In this perspective, we also performed an additional experiment where low-affinity MinE07 was co-incubated with living cells with an approximately 40-fold excess of Cetuximab, a well-known EGFR targeting therapeutic antibody used in clinics (Fig. SN6). No significant difference in the binding of the aptamer was observed in presence of Cetuximab or a control antibody. In fact, the number of detected localizations measured with low-affinity MinE07 was reduced (~20% reduction of signal) with the same extent when co-incubated in presence with Cetuximab or a control polyclonal antibody. This result suggests that the observed reduction in the aptamer binding was most likely due to a steric hindrance created on the plasma membrane during the pre-blocking step performed in presence of the only antibody (either Cetuximab or a control antibody) at high concentration, and thus it was not related to a competition for the binding of EGFR. Our findings are consistent with a previous report, in which flow cytometry assays were performed to assess competition between MinE07 and Cetuximab on A431 cells[27]. Indeed, no competition between these two ligands was observed, suggesting that the epitope recognized by Cetuximab does not overlap with the binding site of MinE07 on EGFR. Thus, MinE07 aptamer and its variants are potentially compatible for the study of EGFR motion, localization and signaling upon treatment with therapeutic drugs, such as Cetuximab.

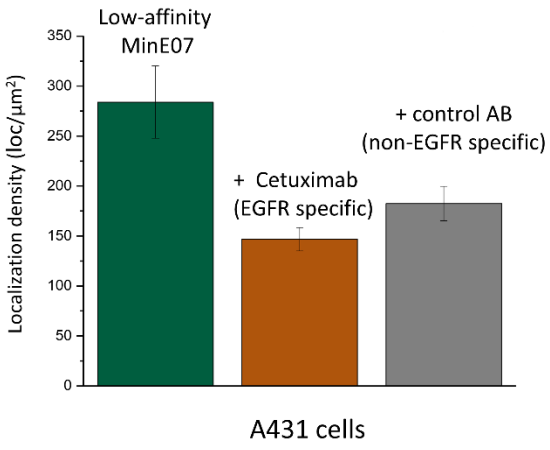

Figure SN6. Comparison of membrane localization densities for living A431 cells exposed to 7 nM low-affinity MinE07. GREEN: cells were just exposed to aptamer probe; ORANGE: cells were pre-blocked with an excess of Cetuximab, washed and then co-incubated with 7 nM aptamer probe and Cetuximab (approximately 40-times in excess); GREY: cells were pre-blocked with an excess of control antibody (anti-human polyclonal), washed and then co-incubated with 7nM aptamer probe and antibody (approximately 40-times in excess);

Supplementary References

[1] D. Porciani, L. N. Cardwell, K. D. Tawiah, K. K. Alam, M. J. Lange, M. A. Daniels, D. H. Burke, *Nat Commun* **2018**, *9*, 2283.
[2] I. F. Sbalzarini, P. Koumoutsakos, *Journal of Structural Biology* **2005**, *151*, 182–195.
[3] M. Ovesný, P. Křížek, J. Borkovec, Z. Švindrych, G. M. Hagen, *Bioinformatics* **2014**, *30*, 2389–2390.
[4] J. Zadeh, C. Steenberg, *Journal of Computational Chemistry* **2011**, DOI 10.1002/jcc.
[5] M. Zuker, *Nucleic Acids Research* **2003**, *31*, 3406–3415.
[6] L. D. Hughes, R. J. Rawle, S. G. Boxer, *PLoS ONE* **2014**, *9*, e87649.
[7] L. C. Zanetti-Domingues, C. J. Tynan, D. J. Rolfe, D. T. Clarke, M. Martin-Fernandez, *PLoS ONE* **2013**, *8*, e74200.
[8] K. Davis, *Nucleic Acids Research* **1998**, *26*, 3915–3924.
[9] L. A. Wheeler, R. Trifonova, V. Vrbanac, E. Basar, S. McKernan, Z. Xu, E. Seung, M. Deruaz, T. Dudek, J. I. Einarsson, et al., *J. Clin. Invest.* **2011**, *121*, 2401–2412.
[10] W. Jin, C. J. Penington, S. W. McCue, M. J. Simpson, *PLoS ONE* **2017**, *12*, e0181941.
[11] R. M. Reilly, R. Kiarash, J. Sandhu, Y. W. Lee, R. G. Cameron, A. Hendler, K. Vallis, J. Gariépy, *J. Nucl. Med.* **2000**, *41*, 903–911.
[12] L. M. Smith, M. J. Birrer, M. R. Stampfer, P. H. Brown, *Cancer Res* **1997**, *57*, 3046.
[13] M.-L. I. E. Harwardt, P. Young, W. M. Bleymüller, T. Meyer, C. Karathanasis, H. H. Niemann, M. Heilemann, M. S. Dietz, *FEBS Open Bio* **2017**, *7*, 1422–1440.
[14] S. Derer, P. Bauer, S. Lohse, A. H. Scheel, S. Berger, C. Kellner, M. Peipp, T. Valerius, *J.I.* **2012**, *189*, 5230–5239.
[15] J. A. M. Berkers, van Bergen en Henegouwen, Paul M. P., Boonstra, Johannes, *J. Biol. Chem.* **1991**, *266*, 922–927.
[16] F. Capuani, A. Conte, E. Argenzio, L. Marchetti, C. Priami, S. Polo, P. P. Di Fiore, S. Sigismund, A. Ciliberto, *Nat Commun* **2015**, *6*, 7999.
[17] M. Ovesný, P. Křížek, J. Borkovec, Z. Švindrych, G. M. Hagen, *Bioinformatics* **2014**, *30*, 2389–2390.
[18] C. Chen, F. Loe, A. Blocki, Y. Peng, M. Raghunath, *Advanced Drug Delivery Reviews* **2011**, *63*, 277–290.
[19] M. Assunção, C. W. Wong, J. J. Richardson, R. Tsang, S. Beyer, M. Raghunath, A. Blocki, *Materials Science and Engineering: C* **2020**, *106*, 110280.
[20] J. S. Kim, A. Yethiraj, *Biophysical Journal* **2010**, *98*, 951–958.
[21] D. Axelrod, M. D. Wang, *Biophysical Journal* **1994**, *66*, 588–600.
[22] N. F. Dupuis, E. D. Holmstrom, D. J. Nesbitt, *Proceedings of the National Academy of Sciences of the United States of America* **2014**, *111*, 8464–8469.
[23] D. Kilburn, J. H. Roh, L. Guo, R. M. Briber, S. A. Woodson, *Journal of the American Chemical Society* **2010**, *132*, 8690–8696.
[24] N. Li, H. H. Nguyen, M. Byrom, A. D. Ellington, *PLoS ONE* **2011**, *6*, e20299.
[25] C. C. Valley, D. J. Arndt-Jovin, N. Karedla, M. P. Steinkamp, A. I. Chizhik, W. S. Hlavacek, B. S. Wilson, K. A. Lidke, D. S. Lidke, *MBoC* **2015**, *26*, 4087–4099.
[26] Y. Sako, S. Minoghchi, T. Yanagida, *Nat Cell Biol* **2000**, *2*, 168–172.
[27] S. Cheng, O. Jacobson, G. Zhu, Z. Chen, S. H. Liang, R. Tian, Z. Yang, G. Niu, X. Zhu, X. Chen, *Eur J Nucl Med Mol Imaging* **2019**, *46*, 948–956.